

Two-Dimensional Transition Metal Dichalcogenides and Metal Oxide Hybrids for Gas Sensing

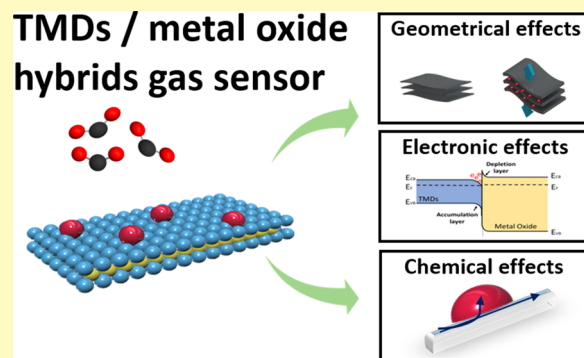
Eunji Lee,[†] Young Soo Yoon,^{*,‡} and Dong-Joo Kim^{*,†}

[†]Materials Research and Education Center, Auburn University, Auburn, Alabama 36849, United States

[‡]Department of Chemical and Biological Engineering, Gachon University, Seongnam 13120, Republic of Korea

ABSTRACT: Two-dimensional (2D) nanomaterials have demonstrated great potential in the field of gas sensing due to their layered structures. Especially for 2D transition metal dichalcogenides (TMDs), inherent high surface areas and their unique semiconducting properties with tunable band gaps make them compelling for sensing applications. In combination with the general benefits of 2D nanomaterials, the incorporation of metal oxides into 2D TMDs is a recent approach for improving the gas sensing performance of these materials by the synergistic effects of the hybridization. This Review aims to comprehend the sensing mechanisms and the synergistic effects of various hybridizations of 2D TMDs and metal oxides. The Review begins with the gas sensing mechanisms and synthesis methods of 2D TMDs. Achievements in recent research on 2D TMDs and their metal oxide hybrids for sensor applications are then comprehensively compiled. To clearly understand the collective benefits of TMDs and metal oxide hybrids, the hybridization effects are discussed in three aspects: geometrical, electronic, and chemical effects.

KEYWORDS: *gas sensor, 2D materials, transition metal dichalcogenides, metal oxide, hybrids, nanocomposite, heterojunction*



A significant upsurge in research interests in two-dimensional (2D) nanostructured materials has arisen, seeking to utilize the extraordinary properties inherent to 2D materials in multiple fields, including energy storage, electronics, and chemical sensing.^{1,2} A 2D nanostructure is defined as a single layer or a few atomic layers of nanocrystalline materials, which structurally exist as nanosheets, nanomembranes, and nanoflakes.³ The 2D nanostructure can generally be classified as either 2D allotropic elements or covalently bonded compounds.⁴ Originating from their atomically thin layers, the 2D nanostructured materials manifest unique chemical and physical characteristics, which show great promise for sensing applications. Specifically, the atomic-scale thickness of a 2D nanomaterial magnifies the surface-to-volume ratio, which exposes more active surfaces to target gases. Van der Waals gaps between the characteristic surface configuration of the layers and thickness-dependent physical and chemical properties are distinct qualities that make 2D nanomaterials outstanding candidates for gas sensors.^{5,6} The ability of 2D nanomaterials to identify gas analytes at room temperature offers the possibility of wearable gas sensors integrated on a flexible substrate.⁷

Among intrinsic 2D materials (graphene,⁸ transition metal dichalcogenides (TMDs),⁹ phosphorene,¹⁰ MXenes,¹¹ etc.), extensively researched graphene and other carbon-based materials are chemically inert, which means that surface functionalization with other molecules is required for gas sensing applications. In contrast, 2D TMDs display versatile chemistry and tunable band gaps that are much more beneficial in the

design of practical gas sensing devices. Layer-dependent properties in conjunction with surface structure modifications such as exposure of particular edge sites, chemical doping, and ligand conjugation were investigated to improve sensing performance of TMDs.¹² However, the rapidly developing field of TMD research still needs to address challenges such as selectivity, gas response, response time, recovery time, and stability. To give a few examples, 2D TMDs may suffer the same selectivity issues as metal oxides by responding to more than one type of gas. The response time of 2D TMDs sensors is sluggish, and recovery is often incomplete. Over time, the surface of layered 2D TMDs can be partially covered by oxygen or moisture in an ambient atmosphere due to different kinetics of adsorption and desorption, which may gradually degrade the sensing performance and long-term stability.¹³ Therefore, more recent efforts to utilize 2D TMDs for chemical sensing has moved to exploration of hybridizing novel metals and/or metal oxides into TMDs with tailored morphology. Previous studies have successfully demonstrated the improved gas sensing performance resulting from the hybridization. Geometrical benefits can be expected to result from integrating metal oxides with various morphologies to facilitate gas diffusion and absorption. Electrical and chemical functionalization of the sensing material can also be obtained by designing heterojunctions.

Received: September 21, 2018

Accepted: October 1, 2018

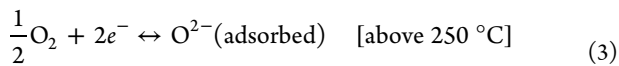
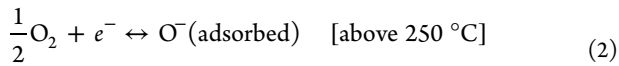
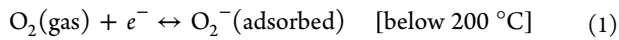
Published: October 1, 2018

Although several reviews of 2D TMDs^{14,15} and 2D materials for gas sensing^{3,5,16–19} have been published recently, no review has focused on TMDs and metal oxide hybrids. Additionally, the improved sensing performance resulting from the hybridization has been verified through recent results, but the mechanisms that lead to these remarkable effects have not been clearly discussed. Therefore, herein we comprehensively review the literature of 2D TMDs and their metal oxide hybrids to understand the fundamental mechanisms and current progress in the field of gas detection. In this Review, we present the reported mechanisms of TMDs and metal oxides for the basic understanding of each material. The unique gas sensing characteristics of selected 2D TMDs and their hybrids are then discussed. Lastly, the challenges and future directions to develop hybrids-based sensors will be addressed with a full summary. This critical review will provide great insight into the evolution of TMD materials and their metal oxide hybrids to unravel the complications of hybridization.

GAS SENSING MECHANISM

Two-Dimensional Transition Metal Dichalcogenides. The basic principle of gas sensing in 2D TMDs is mainly based on the charge-transfer processes between gas molecules and the surface of sensing materials. Different from the conventional metal oxides, the 2D materials act as a charge acceptor or donor, resulting in the resistance (or conductance) change of the overall system. Once exposed to reactive gases, gas molecules are absorbed on the surface of 2D materials by the electrostatic force. The direction of electron charge transfer is determined by the type of reactive gas, either reducing or oxidizing. The resistance of the sensing material is recovered up to its initial value due to desorption of gas molecules upon exposure to air. The amount of resistance modulation is determined by the charge affinity of reactive gas to release or withdraw electrons. Using a p-type 2D material as an example, the resistance of the sensing material usually increases under the exposure of reducing gases.

Metal Oxides. The working principle of metal oxide sensors has been extensively studied. The sensing mechanism of the conventional metal oxide sensors is related to adsorbed oxygen ions on the oxide surface. The oxygen ions are formed by drawing electrons from the conduction band of the metal oxide, and different forms are possible depending on the operating temperature.^{20,21} Below 200 °C, electrons are attached to oxygen molecules as shown in eq 1. Above 250 °C, the oxygen molecules are dissociated into oxygen ion atoms with electric charge by pulling electrons from metal oxide as shown in eqs 2 and 3.



The interaction between the oxygen ions and gas analytes can be divided into two main categories depending on the majority carrier, electrons or holes. When the majority carriers are electrons, the metal oxide is considered to be n-type, while the majority carriers are holes in the p-type metal oxide sensors. Using n-type metal oxides as an example, the electrons in the conduction band of the metal oxide are decreased due to the reactions of eqs 1–3, resulting in increased resistance at the operating temperature. Once the target gas is introduced,

the electrons from the reducing gas are transferred to the conduction band of the metal oxide causing the resistance of the sensor to decrease. It should be noted that the opposite resistance change occurs with an oxidizing gas. The categorized sensing behavior of n-type and p-type sensing materials to reducing and oxidizing gases is compared elsewhere.²² As an example, NO_x is considered as an oxidizing gas due to unpaired electrons around the N atom, while NH₃ acts as a reducing gas due to its lone electron pair.⁵ Due to the dominant role of oxygen ions, the metal oxide sensors are typically operated at elevated temperatures.

GAS SENSING PROPERTIES OF 2D TRANSITION METAL DICHALCOGENIDES

TMDs are MX₂-type inorganic compounds where M is a transition element such as Ti, Zr, Hf, V, Nb, Ta, Mo, W, Tc, or Re in groups IV, V, and VI of the periodic table, and X is an element of the chalcogen species such as S, Se, or Te. When reduced to a single layer or a few layers, the TMDs have shown excellent electric properties comparable to those of graphene.²³ The 2D layered structure of TMDs consists of strong molecular intralayer bonds and weak van der Waals interlayer bonds. The weak interlayer bonding allows exfoliation of TMDs down to single layers or multilayers by using mechanical exfoliation or electrochemical intercalation.¹⁴ In general, the thickness of layered TMDs is about 6–7 Å, and the length of M–M bond is typically between 3.15 and 4.03 Å, depending on the size of the metal and chalcogen atoms.²⁴ Higher specific surface area and functionalities driven by such structure make 2D TMDs promising candidates for sensor applications.

The electronic and magnetic characteristics of TMDs hinge on the coordination number of the transition metal and its d-electrons. The transition metal (M) atoms in TMDs have four electrons to fill the bonding states and chalcogen (X) atoms have an oxidation state of -2. Thus, the number of d orbital electrons will vary 0 to +6, which influences electronic properties. The electrical nature of TMDs can be tuned from semiconductors (MoS₂, MoSe₂, WS₂, WSe₂, ...) to metallic (NbTe₂, TaTe₂, ...) or superconductors (NbS₂, NbSe₂, ...). The partially filled d-orbitals in transition metals provide metallic conductivity, while fully filled d-orbitals give semiconducting properties. The surface of layered TMDs is terminated by chalcogen atoms with lone-pair electrons. The absence of dangling bonds in TMDs stabilizes the material against ambient environment and gives high mobility in compliance with the substrates and metal contacts. For instance, the mobility of molybdenum disulfide (MoS₂) is about 700 cm⁻¹ V⁻¹ s⁻¹ on SiO₂/Si substrate at room temperature.²⁵ An important attribute of TMDs for gas sensing can be a tunable band gap. Graphene, a popular 2D material, is metallic with a zero band gap, but several TMDs such as molybdenum disulfide (MoS₂), tungsten disulfide (WS₂), and tin disulfide (SnS₂) have a direct and indirect band gap around 1–2 eV due to their low intrinsic carrier concentration. The fascinating electrical and optical properties of TMDs arise from the transition of an indirect band gap to a direct band gap as the thickness changes from bulk to monolayer due to quantum confinement. Moreover, mechanically flexible and strong TMDs can be another advantage to extend fields of chemical sensors. It is reported that few-layered MoS₂ has a high Young's modulus of 0.33 ± 0.07 GPa that outperforms the stainless steel and graphene oxide.²⁶

In the TMD class, disulfides such as MoS₂, WS₂, and SnS₂ are great representatives of TMDs for chemical sensing. The crystal

Table 1. Density Functional Theory Calculation of Adsorption Energy and Charge Transfer for 2D Materials

		NH ₃	H ₂ O	NO ₂	NO	CO	O ₂	H ₂	ref
graphene	E_{ad} (eV)	0.031	0.047	0.067	0.029	0.014	—	—	38
	ΔQ (e)	0.027	-0.025	-0.099	0.018	0.012	—	—	
MoS ₂	E_{ad} (eV)	-0.250	-0.234	-0.276	-0.195	-0.128	-0.106	-0.07	39
	ΔQ (e)	-0.069	0.012	0.100	0.011	0.020	0.034	0.004	
WS ₂	E_{ad} (eV)	—	-0.18	—	—	-0.14	-0.11	—	40
	ΔQ (e)	—	0.0048	—	0.0096	0.0078	0.0134	—	
MoTe ₂	E_{ad} (eV)	0.13	—	0.2	—	—	—	—	41
	ΔQ (e)	—	—	—	—	—	—	—	

structure of molybdenum disulfide (MoS₂) has been revealed for more than 5 decades, but its electrical and optical features have been investigated recently.²⁷ In each layer of MoS₂, Mo atoms are sandwiched between covalently bonded S atoms, with a layer height of about 0.65 nm. The crystal structure of MoS₂ with a trigonal prismatic arrangement manifests as hexagonal crystal structure.²⁸ Monolayers of MoS₂ have a direct band gap of 1.8 eV, while bulk (>8 layers) MoS₂ presents an indirect band gap of 1.29 eV. Unique physical and chemical features of MoS₂ for gas sensors include a layer-dependent band gap, a high surface-to-volume ratio, and a high adsorption coefficient. Tungsten disulfide (WS₂) is another TMD material. The structure of WS₂ is similar to MoS₂, where tungsten layers are sandwiched in between two sulfur layers in a trigonal prismatic arrangement. It is reported that a single layer of WS₂ has a direct band gap with a theoretical value of 1.8–2.1 eV.¹⁵ For gas sensing applications, WS₂ can be more attractive than MoS₂ because WS₂ has ambipolar field-modulation behavior²⁹ and high electron mobility at room temperature up to 234 cm²/(V·s).³⁰ In addition, the higher photoluminescence (PL) emission efficiency of monolayered WS₂ suggests a higher quantum efficiency than MoS₂ crystals.³¹ Other types of 2D TMDs such as molybdenum diselenide (MoSe₂) and molybdenum ditelluride (MoTe₂) have also similar structural characteristics to MoS₂ and WS₂. The atomic structure of single-layer MoSe₂ is larger due to the larger atomic radii of the Se atoms compared to Sn. In a single layer of MoSe₂, the length of the Mo–Se bond is 2.53 Å, and the length of the Se–Se bond is 3.29 Å.³² The indirect band gap of bulk MoSe₂ is about 1.1 eV, while the direct band gap of the single layer is about 1.55 eV.³³ A recent experiment has revealed that the mobility of MoSe₂ is ~50 cm²/(V·s) at room temperature.³⁴ Interestingly, MoTe₂ has larger bond length and lower binding energy than other TMDs, which drives its potential to improved gas sensitivity.³⁵ Although tin does not belong to transition metal category, tin disulfide (SnS₂) formed a 2D layered phase with hexagonal structure similar to TMDs.³⁶ It is interesting to note that larger electronegativity of SnS₂ in comparison with other TMDs may suggest a high absorption ability corresponding to a high gas response. However, the relatively stronger temperature dependency of SnS₂ on electronic band structure may need consideration to determine optimal sensing temperature based on understanding absorption and recovery of kinetics at different temperatures.³⁷

Each 2D material presents different electrical features and surface configurations, which influence their gas sensing properties. Another important interpretation of gas sensing property in 2D TMDs can be conducted by understanding the charge-transfer mechanism depending on their surface

configuration and electrical characteristics. The interactions between sensing materials and gas molecules can be inferred by the adsorption energy and the amount of charge transfer, which are commonly evidenced by first-principles calculations based on density functional theory (DFT). Such computational simulations were able to consider parameters including adsorption positions and orientations of gas molecules on a 2D material. Table 1 gives the results of the DFT simulations on the most stable adsorption position and orientation. Absorption energy between 2D materials and gas molecules was calculated by eq 4.⁴²

$$E_{ad} = E_{(2D+gas)} - [E_{(2D)} + E_{(gas)}] \quad (4)$$

where $E_{(2D+gas)}$ is the total energy of a supercell containing both a 2D material and a gas molecule, $E_{(2D)}$ is the total energy of the 2D sensing material, and $E_{(gas)}$ is the total energy of a supercell containing a gas molecule. Here, the negative value of E_{ad} indicates an exothermic reaction, meaning thermodynamically favorable reaction. The negative value of ΔQ means the direction of charge transfer from gas molecules to sensing material or vice versa at the optimal adsorption configuration. The large value of adsorption energy can be interpreted as the level of selective response to the gas molecule over other species.⁴³ The amount of ΔQ can be associated with the number of transferred electrons between gas molecules and the sensing material. In addition, physisorption and chemisorption can be determined from ΔQ value.

Table 2 summarizes recent examples in gas sensing performance using the 2D TMD nanostructured materials. The performance of gas sensors is evaluated by gas response, selectivity, stability, response time, and recovery time. In general, the gas response is calculated by the ratio of resistance R_g/R_a or R_a/R_g to have responding value greater than 1. Alternately, $\Delta R/R_a$ is also used to measure the resistance difference before and after gas injection ($\Delta R = |R_g - R_a|$), where R_g and R_a are the resistance of gas sensors with target gas and the resistance of gas sensors in ambient air, respectively. The response time is commonly defined as the time spent to reach 90% of the gas response in the presence of a target gas. Similarly, the recovery time is defined as the time spent to return to 90% of initial status without gas molecules.¹⁶ The sensing performance of the representative TMDs including MoS₂, WS₂, MoSe₂, MoTe₂, and SnS₂ was listed in Table 2. Since most literature uses NH₃ and/or NO_x for evaluation of sensing properties, the results were compared in terms of NH₃ and/or NO_x gas.

Molybdenum Disulfide (MoS₂). The gas sensing mechanism based on the charge transfer in atomic layered MoS₂ was elucidated using in situ PL by Cho et al.⁴² In situ PL spectra of

Table 2. Literature Study on Gas Sensing Performance of 2D Nanomaterial Gas Sensors Working at Room Temperature

material	thickness	analyte	concentration	gas response, $\Delta R/R_a$ (%)	limit of detection	response/recovery time (min)	ref
MoS ₂	atomic layer	NO ₂	5 ppm	15	—	—/—	42
	atomic layer	NH ₃	1 ppm	1	5 ppm	—/—	44
	single layer	NO ₂	120 ppb	35	120 ppb	—/—	45
	2 layers	NO ₂	1.2 ppm	6.1	2 ppb	—/—	46
	2 layers	NO	2 ppm	80	0.8 ppm	—/—	47
	5 layers	NO ₂	1 ppm	2.6	1 ppm	11.3/5.3	47
	20 nm	NO ₂	100 ppm	30	10 ppm	—/—	9
	20 nm	NH ₃	2 ppm	0.01	300 ppb	—/5	48
WS ₂	2–50 nm	NH ₃	5 ppm	0.02	1.4 ppm	—/—	49
	110 nm	NH ₃	5 ppm	1.6	1 ppm	—/—	50
	1–44 layers	NH ₃	250 ppm	2.6	50 ppm	—/—	51
	multilayers (5 nm)	NO ₂	5 ppm	68.4	0.1 ppm	—/—	52
MoSe ₂	single layer	NH ₃	300 ppm	300	50 ppm	2.5/9	32
MoTe ₂	few layers	NO ₂	100 ppb	8	12 ppb	—/—	41
SnS ₂	1–3 layers	NH ₃	100 ppm	2.13 ^a	20 ppm	—	53

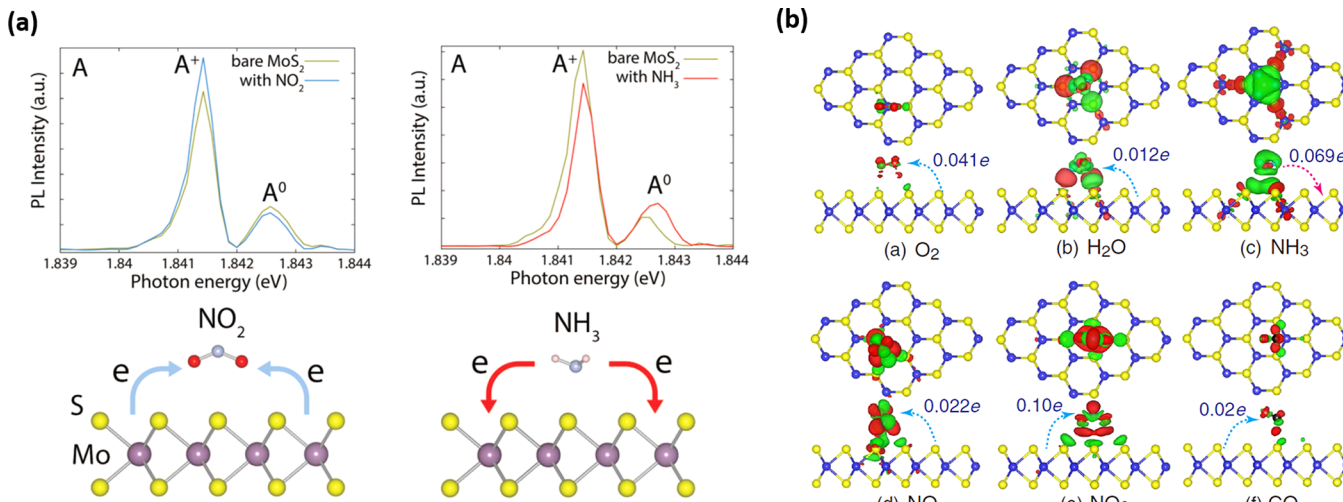
^a I_g/I_0 .

Figure 1. Photoluminescence and charge density of MoS₂ to n-type (NH₃) and p-type (NO₂) dopants. (a) In situ PL spectra recorded from the MoS₂ with NO₂ and NH₃ molecules. (b) Charge density difference plots to O₂, H₂O, NH₃, NO, NO₂, and CO on monolayer MoS₂. The red (green) distribution corresponds to charge accumulation (depletion).

the MoS₂ were recorded in the presence of NO₂ (p-type dopant) and NH₃ gas (n-type dopant). The relatively low-energy A exciton was separated into a trion of A^{-/+} depending on the majority charge carrier and a neutral exciton of A⁰. For bare MoS₂, the positive trion peak (A⁺) of PL spectra was dominant, indicating a p-type characteristic of MoS₂ on SiO₂/p⁺Si substrate in Figure 1a. After NO₂ exposure, the A⁺ peak was increased and the A⁰ peak was decreased, showing trade-off phenomena. A neutral exciton (A⁰) was converted to a quasi-particle (A⁺) owing to hole injection from NO₂ (electron extraction from MoS₂) while the opposite tendency was observed when NH₃ (electron injection from NH₃) was introduced. The in situ PL results experimentally confirmed the charge-transfer mechanism of atomic layered MoS₂. Theoretical studies have shown to support the charge-transfer mechanism. Yue et al.³⁹ computed the adsorption energy and the amount of charge transfer between monolayer MoS₂ and various gas molecules, O₂, H₂O, NH₃, NO, NO₂, and

CO using first-principles (Figure 1b). DFT calculations revealed that these gas molecules are physically absorbed onto the MoS₂ with small charge transfer, acting to inject or extract electrons. During the physical absorption of the gas molecules, the band structure of MoS₂ was not significantly changed, although several gases created adsorbate states in the band gap of MoS₂. In theoretical aspect, TMD materials can be more favorable than graphene for gas absorption. As listed in Table 1, E_{ad} of MoS₂ to all gas molecules exhibits a negative value, while graphene does positive. The negative E_{ad} of MoS₂ suggests that gas molecules are voluntarily absorbed on the surface of MoS₂, with transferring or withdrawing electrons with the amount of ΔQ .

Much effort has been dedicated to enhancing gas sensing performance of bare MoS₂, by tailoring the number of layers and adjusting their alignment. The effect of the number of MoS₂ layers on the gas sensing performance was studied by He et al.⁴⁵ The thickness of MoS₂ layers was controlled by the volume of

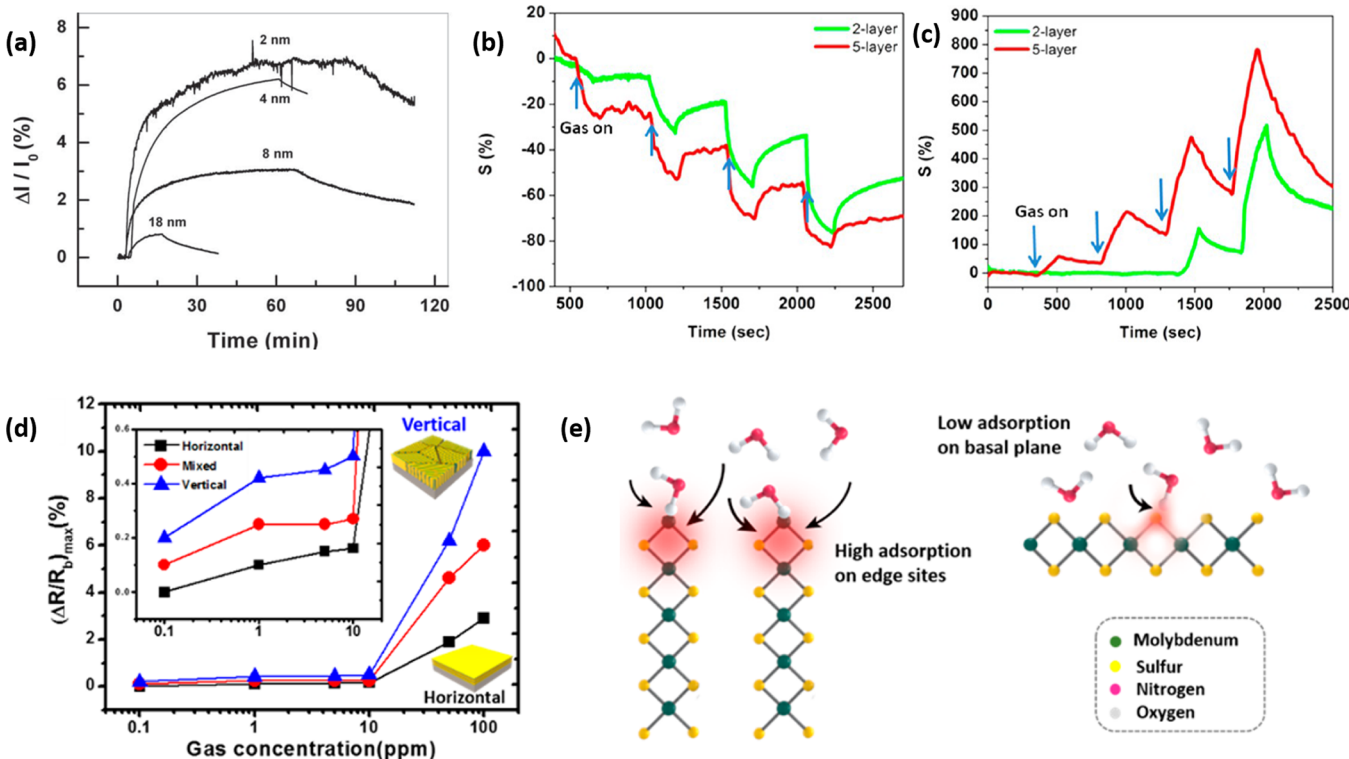


Figure 2. (a) Detection of 1.2 ppm of NO₂ using a MoS₂ thin film transistor on PET with different thickness of MoS₂ thin film. (b) Comparative two- and five-layer MoS₂ cyclic sensing performances with NH₃ for 100, 200, 500, and 1000 ppm. (c) Comparative two- and five-layer MoS₂ cyclic sensing performances with NO₂ for 100, 200, 500, and 1000 ppm. (d) Resistance response upon exposure to NO₂ gas with concentrations ranging from 0.1 to 100 ppm. (e) Schematic illustration of gas adsorption mechanism on edge sites and basal plane of MoS₂.

MoS₂ solution during a spin-coating process, and the conductance of the prepared MoS₂ was measured with and without NO₂ and NH₃ gases. Regardless of MoS₂ layer thickness, the conductance of MoS₂ channels was increased when NO₂ gas was injected, showing p-type characteristics. In Figure 2a, the gas response to NO₂ was reduced with increasing thickness of MoS₂ layers ranging from 2 to 18 nm since the surface-to-volume ratio of the MoS₂ channel was decreased with increasing thickness. Late et al.⁹ prepared two- to five-layered MoS₂ on a SiO₂/Si substrate whose thickness is ranging from 1.4 to 3.3 nm (Figure 2b,c). The five-layer MoS₂ film (3.3 nm) has shown the highest gas response to both NO₂ and NH₃. The authors argued different electronic structures such as the level of the conduction and valence bands of MoS₂ responsible for better sensing properties. However, a clear explanation on the specific sensing mechanism was not given to clarify the opposite tendency of thickness dependence of gas response. Besides the number of layers, the alignment of 2D layered MoS₂ also has an impact on the sensing properties. Cho et al.⁵⁴ have demonstrated enhanced gas adsorption properties of MoS₂ layers by vertically aligning the layer direction. In their work, Mo seed layers were pre-deposited on SiO₂ and converted to MoS₂ film by sulfurization during the chemical vapor deposition (CVD) process. The growth direction of CVD grown MoS₂ was varied according to the thickness of the Mo seed layer, and three different alignments of MoS₂ were prepared, horizontal, mixed, and vertical orientations. Their sensing properties of MoS₂ on NO₂ and NH₃ showed the highest gas response from vertically aligned MoS₂, and the lowest from the horizontal one (Figure 2d). The result is due to higher absorption on edge sites of MoS₂ than basal plane sites, which arise from the high d-orbital electron density of Mo

(Figure 2e). Therefore, both geometric alignment of 2D layers and layer thickness should be considered to improve gas sensing properties.

Tungsten Disulfide (WS₂). Similar to MoS₂, the factors such as the number of layers and alignment affect the gas sensing performance of WS₂. Qin et al.⁵¹ studied the relationship between the number of WS₂ layers and sensing performance. WS₂ samples with different thicknesses were prepared by an exfoliation ranging from one layer to bulk. By increasing the number of layers, the gas response becomes larger due to more gas molecules inserted into their inner layers and interacted with the two adjacent layers (Figure 3a). However, longer recovery time was required in thicker layers since desorption became more difficult. The results can be explained from the first-principles calculations. The estimated binding energy between NH₃ molecules and single layer of WS₂ is -0.179 eV, implying a weak van der Waals interaction. On the other hand, the binding energy of NH₃ molecules inside the interlayer is much stronger at -0.356 eV resulting from the top and bottom dual interaction of WS₂ layers, which leads to longer recovery time. As studied with MoS₂ on surface functionalization,⁵⁴ WS₂ edge-functionalized carbon nanofibers (CNFs) with multiple tubular pores (WS₂@MTCNFs) on gas sensing properties were investigated by Cha et al.⁵⁵ More edge of WS₂ nanoflakes was functionalized on the surface with CNFs structures, and higher specific surface area was obtained from MTCNFs, which improved gas sensing response (Figure 3b). However, the effect of surface area is diminished as the concentration of NO₂ decreases, suggesting a relatively minor influence of a porous structure at low levels of concentration. The selectivity toward NO₂ also improved against interference of NH₃ and toluene (C₇H₈) (Figure 3c).

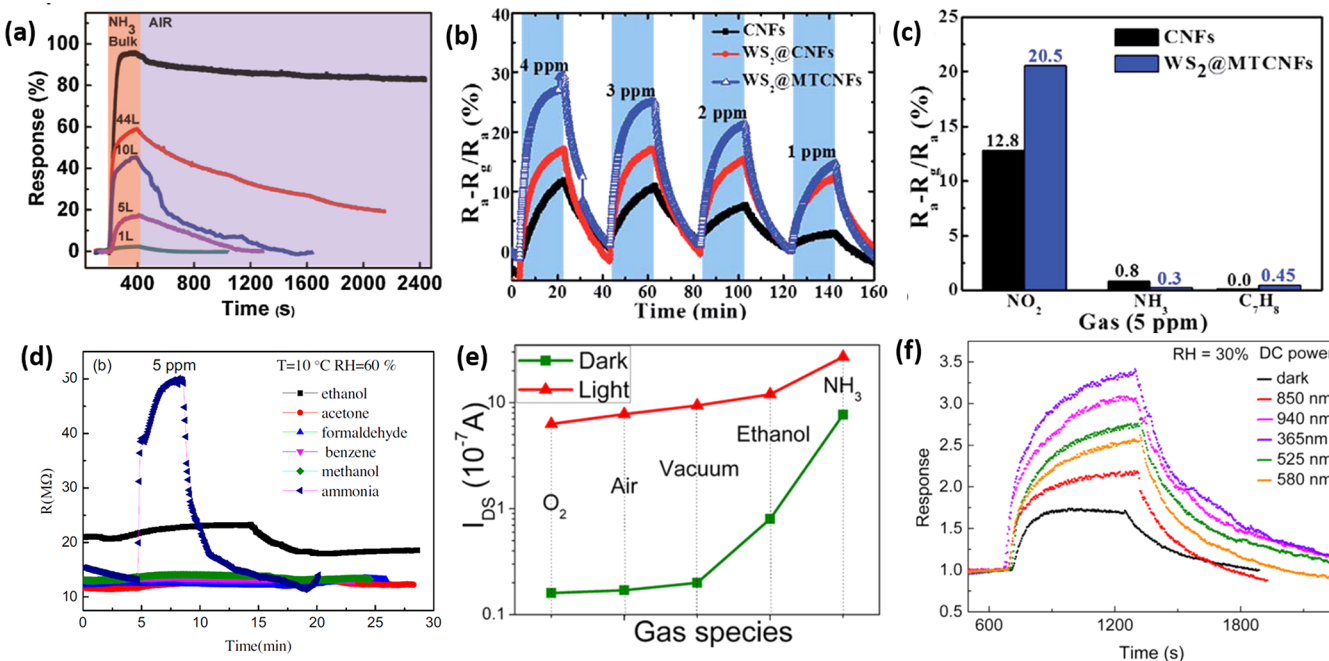


Figure 3. (a) Response—recovery curves of thin WS₂ nanosheets and bulk WS₂ interaction with 250 ppm of NH₃ at room temperature. (b) Dynamic response transients of CNFs, WS₂@CNFs, and WS₂@MTCNFs to NO₂ in the concentration range of 1–4 ppm at room temperature. (c) Selective property of CNFs and WS₂@MTCNFs toward 5 ppm of NO₂, NH₃, and C₇H₈. (d) The selectivity of the WS₂ nanoflake-based sensor to different gases at RH = 60%. (e) The extracted dark current and photocurrent under different gas atmospheres. (f) Response curves of the WS₂-based chemiresistive sensors under different light illuminations driven by DC power to 10 ppm of NH₃.

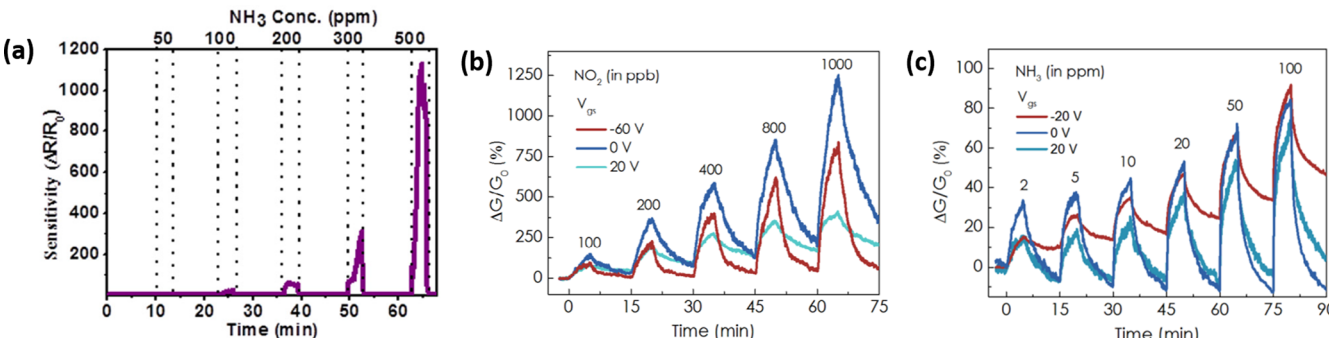


Figure 4. (a) NH₃ sensing response of single-layer MoSe₂ as a function of gas concentration. (b) Real-time conductance change of p-type MoTe₂ FET sensor upon exposure to different concentrations of NO₂ under different gate biases. (c) Real-time conductance changes of n-type MoTe₂ FET sensor to different concentrations of NH₃ under different gate biases.

The enhanced selectivity of WS₂-edge-functionalized CNFs may originate from the high density of WS₂ edges that preferentially react with NO₂ gases. Apart from NO₂ analyte, pure WS₂ showed selective response toward ammonia⁵⁰ in Figure 3d.

In addition to structural modulation of layered WS₂, external factor such as light illumination was investigated. Huo et al.⁵⁶ reported that the charge transfer between the WS₂ nanoflakes and the physical-adsorbed gas molecules is closely related to the photoelectrical features of WS₂ (Figure 3e). The source–drain current of the WS₂ transistor device is slightly decreased in O₂ and largely increased in ethanol and NH₃. Under the light exposure, all gas molecules can be further absorbed due to photoresponsivity and external quantum efficiency. The dynamic response by light can be ascribed to two physical mechanisms; the photogeneration/recombination of electron–hole pairs and charge transfer.⁵⁷ Figure 3f displays the response of the WS₂ to 10 ppm of NH₃ under different light illuminations, from infrared (IR) to ultraviolet (UV), at 40 °C with a relative humidity (RH)

of 30%. The response of the multistacked WS₂ was enhanced under the overall range of light due to the photosensitive natures of the samples. Under the illumination of 365 nm light, the response of WS₂ to NH₃ was at the maximum of 3.4 (R_g/R_a) with the shortest response and recovery time of 252 and 648 s compared to the other range of the lights. This result suggests light modulation should be a great option to improve the sensing performance of TMDs.

Other TMDs: Molybdenum Diselenide (MoSe₂) and Molybdenum Ditelluride (MoTe₂). The first demonstration of a gas sensor device based on single-layer MoSe₂ was reported by Late et al.³² Single-layer MoSe₂ exfoliated from bulk MoSe₂ was fabricated on a SiO₂ substrate using electron beam lithography. The gas response of the MoSe₂ sensor was increased with higher NH₃ concentrations at room temperature⁹ (Figure 4a). The gas response value of MoTe₂ was comparable with that of MoS₂, but the response time (2.5 min) and recovery time (9 min) were slightly shorter. The first principle calculations reported

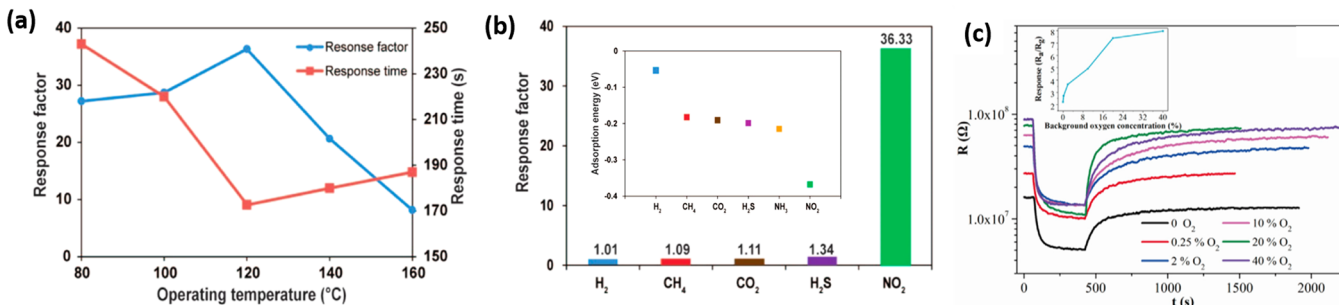


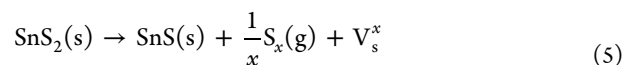
Figure 5. (a) Response factor and response time of sensors made of 2D SnS₂ flakes in the presence of 10 ppm of NO₂ in synthetic air balance as a function of operation temperatures. (b) Measured cross-talk of 2D SnS₂ flakes toward H₂ (1%), CH₄ (10%), CO₂ (10%), H₂S (56 ppm), and NO₂ (10 ppm). (Inset shows the calculated molecule–surface adsorption energies of 2D SnS₂ flakes toward the gases together with NH₃.) (c) Response–recovery characteristics of the SnS₂ based sensor to 100 ppm of NH₃ in different background oxygen contents at 200 °C. (Inset shows the corresponding response curve.)

that MoSe₂ can be sensitive to NO₂ due to its large adsorption energy.⁵⁸ Such gas adsorption also strongly influences the electronic characteristics of monolayer MoSe₂ by inducing impurity levels at near Fermi energy. For example, NO₂ has a larger absorption energy than NO and SO₂, which guides that MoSe₂ is more sensitive to NO₂.

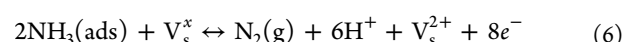
Gas sensors based on MoTe₂ were investigated by Feng et al.⁵⁴ Few-layered MoTe₂ flakes (6.5 nm) were exfoliated from a semiconducting 2H-MoTe₂ bulk and transferred onto SiO₂/n⁺-doped Si substrates. Figure 4b,c shows the conductance change of p-type MoTe₂ field effect transistor (FET) upon the exposure of NO₂ and NH₃ at different concentrations. Interestingly, varying gate biases on the MoTe₂ FET was conducted to investigate recovery kinetics. The MoTe₂ sensor displayed an excellent recovery time of below 10 min, in comparison to graphene and MoS₂ whose recovery times were longer than 1 h at room temperature.^{59,60} At zero bias, the recovery time in NH₃ was shorter than that in NO₂ because of the lower binding energy of NH₃ on MoTe₂ surface. This result showed good agreement with DFT calculations where the binding energy of MoTe₂ is 0.2 eV to NO₂ and 0.13 eV to NH₃. The smaller binding energies of MoTe₂ to NH₃ and NO₂ enable efficient desorption of gas molecules on the surface of MoTe₂ at low thermal energy. These experimental and theoretical results support that both MoSe₂ and MoTe₂ can be great candidates for chemical sensing applications.

Metal Dichalcogenide: Tin Disulfide (SnS₂). The physisorption-based sensing properties of SnS₂ were reported by Ou et al.³⁷ Few-layered 2D SnS₂ flakes were synthesized via a facile wet chemical route with the average thickness of 6 nm. Figure 5a displays that the response factor (R_g/R_a) and gas response time to 10 ppm of NO₂ at an elevated temperature of 80 to 160 °C. The adsorption of NO₂ gas molecules onto the SnS₂ surface was promoted by increasing the operating temperature to 120 °C, and the highest gas response value of 36 was observed at 120 °C. The extrapolated detection limit of SnS₂ toward NO₂ determined from 0.6 to 10 ppm was estimated to be 20–30 ppb. High response was only obtained from NO₂, indicating a strong selectivity to NO₂ over H₂, CH₄, CO₂, and H₂S (Figure 5b). In the DFT calculation, the expected physisorption energies of SnS₂ flakes to NO₂, NH₃, H₂S, CH₄, CO₂, H₂ and O₂ in a 3×3×1 supercell are -0.367, -0.215, -0.199, -0.191, -0.053, 0.182, and 1.430 eV, respectively. These values describe that NO₂ has the greatest adsorption energy, indicating better selectivity of SnS₂ sensor toward NO₂.

The sensing performance of layered SnS₂ can be tuned by controlling defect structure. Qin et al.⁵³ reported that the exfoliated SnS₂ sensor exhibits excellent ammonia sensing while the bulk SnS₂ sensor does not respond. Such observation can be explained in terms of the carrier mobility, high surface-to-volume ratio, and excellent shielding noise natures of 2D SnS₂ material.^{61,62} The sulfur vacancies of the exfoliated SnS₂ serve as the major gas absorption sites with high binding energy because of their high activity, catalysis and dissociation characteristics. The vacancy assisted gas absorption was proven through the DFT calculations.⁶³ Although the formation energy of the S-vacancy system is not thermodynamically favorable, the formation of S-vacancies is unavoidable during the synthesis process, which can enrich the gas adsorption on the host monolayer. The simulation results also help to predict types of gas adsorption. H₂S and CO molecules were physisorbed on S-vacancies in the SnS₂ monolayer, whereas NH₃, NO, and NO₂ molecules were chemisorbed via strong covalent bonds. The effect of background oxygen content on the gas sensing performance also supports the role of S-vacancies.⁶⁴ Figure 5c describes the influence of ambient oxygen concentration on the response of the SnS₂ nanoflowers at 200 °C. The increased sensing response at higher oxygen concentration is explained in terms of the catalytic redox reaction of NH₃. To confirm the experimental result, the molecule–surface adsorption energy of the SnS₂ nanoflowers to NH₃ was calculated with considering oxygen molecules. The binding energy calculation indicates that the increased physisorption energy between NH₃ molecules and SnS₂ may result from the O₂ gas facilitating the adsorption of NH₃. Consequently, the sensing mechanism of the SnS₂ can have two routes in terms of the existence of oxygen. In absence of oxygen, the SnS₂ is dissociated, forming S vacancies at high temperature as shown in eq 5:



where $x = 2\text{--}8$, which represents various S species determined during this process, and V_s^x represents neutral sulfur vacancy. In an anaerobic environment, NH₃ reacts with the sulfur vacancies in the SnS₂ and generates electrons, resulting in a decrease of resistance as shown by eq 6:



In the presence of oxygen at elevated temperature, oxygen absorbed on the surface of SnS₂ takes electrons from the SnS₂, creating a resistance increase. With oxygen involvement, the

response is enhanced because the reaction or gas adsorption between ammonia and oxygen is much easier than that between ammonia and the sulfur vacancies. It appears that the selective sorption by defect structure is a considerable factor in addition to their structural and compositional design for sensor applications of TMDs.

GAS SENSING PROPERTIES OF 2D NANOSTRUCTURE MATERIALS AND METAL OXIDE HYBRIDS

The reported results have demonstrated promising potential of 2D TMDs for gas sensor application, but the experimental results on the sensing performance of the 2D TMDs have not been as high as their theoretical values. Such discrepancy can result from the restacking or aggregating of nanosheets due to the electrostatic force between each pair of layers, which influences a reduced gas response by depleting the number of reaction sites. Therefore, strategies to prevent restacking of 2D TMDs layers are devised, including the formation of hierarchical structures,^{65,66} incorporation of nanomaterials, and novel metal doping.^{67,68} These methods provide improved sensitivity, but the sensors still have a deficiency in selectivity by responding to more than one analyte gas. A possible approach to improve selectivity is to design an electronic nose, an array of single chips to identify several gases simultaneously. In a single unit, decoration or doping of novel metals such as platinum, palladium, silver, and gold, could be a reasonable solution to increase the selectivity via catalytic activities. The use of novel metals improves gas sensing performance by lowering the activation energy because of electronic sensitization and spillover effects.⁶⁹ Some novel metals have a high affinity for specific gas species. Catalyzing the dissociation of O₂ subsequently spills out O⁻ ions onto the surface of the metal oxide, which results in an increased response and faster reaction time.⁷⁰ However, the cost of novel metal and its catalytic poisoning largely offset its merit. Not only selectivity and response, but also long-term stability of the 2D TMD sensor is another critical issue. When 2D TMDs are tightly bound with oxygen molecules in ambient atmosphere, their sensing properties have not been maintained for extended periods of time.^{13,71} To overcome the problem, the application of external energy such as thermal energy or UV energy was attempted to eliminate oxygen molecules by breaking their bonds.⁷²

As an alternative approach to enhance selectivity and sensitivity for an array, the integration of TMDs with metal oxides can be considered for multiple benefits. This combination may solve several challenges including sensitivity, selectivity, and stability issues. Based on the material features of TMDs and metal oxides, the advantages and disadvantages of each material for gas sensing applications are listed in Table 3.⁷³

Table 3. Advantages and Disadvantages of TMDs and Metal Oxide Sensors

TMDs	metal oxide
Advantages	
high electron mobility at low temperature	short response time
low energy consumption	low cost
high gas response	long-term stability
good compatibility	scalable fabrication
mechanical flexibility	
Disadvantages	
low selectivity	low electron mobility at low temperature
sluggish recovery	high operating temperature
relatively high cost	high power consumption
lack of long-term stability	low gas response
lack of scalable fabrication	

It should be noted that these advantages and disadvantages of each classification are not absolute for either category. Rather, they are comparative features that provide reasonable options when designing a gas sensor. With their combination, the agglomeration of TMD nanosheets can be avoided. The resulting porous structure exposes much more surface of TMDs, providing a higher chance to interact with gas molecules. More importantly, the hybrid nanostructure can enhance the gas sensing performance by organizing a heterojunction at the interface between the two materials with a creation of either an n/p-type nanostructure or an n/n- or p/p-type structure. After building contact between two semiconducting materials, the Fermi levels across the interface will be equilibrated to the same energy state. Charge carriers will be transferred, and depletion or accumulated layers will be generated at a heterojunction. Thereupon, electrical features of the hybrids can be tuned toward the significant improvement of gas sensing properties.

The collective benefits of TMDs and metal oxides hybridization can be broken down into three general aspects: geometrical effects, electronic effects, and chemical effects:²²

- Geometrical effects
 - (1) The construction of a hierarchical structure prevents the agglomeration or restacking of 2D TMD nanosheets or metal oxides, which enlarges the active surface area for reaction with analytes.
 - (2) The porous and controlled nanostructure by the incorporation of metal oxides to 2D TMDs during the synthesis facilitates gas absorption and diffusion corresponding to fine-tuning of the metal oxide gas response.
- Electronic effects
 - (1) The potential energy barrier and charge carrier depletion zone at the heterojunction can be modulated by gas adsorption and desorption to act as additional reaction sites.
 - (2) The built-in internal electric field formed at the interface promotes additional oxygen adsorption and charge carrier's conveyance.
 - (3) The depletion zone of charge carriers at the heterojunction acts as a passivation layer to prevent the interaction between atmospheric oxygen and TMDs.
- Chemical effects
 - (1) The chemical bonds created between 2D TMDs and metal oxides can act as efficient charge transport bridges during the gas sensing process.
 - (2) The density of chemisorbed oxygen on the surface of metal oxides can be increased by the interfacial chemical bonds.
 - (3) The receptor function of metal oxides can improve selective adsorption of analytes.

Predicated upon these synergistic effects, the hybrids can be considerably developed, but little work has been done regarding gas sensing properties of TMD/metal oxide hybrids as compiled in Table 4.

A similar effect of hybridization in graphene and metal oxide hybrids was assumed in TMD systems.^{69,73} Metal oxides such as tin oxide (SnO₂), zinc oxide (ZnO), and tungsten oxide (WO₃) with various nanostructures have been incorporated to 2D TMDs mostly by hydrothermal or layer-by-layer methods. Through the hybridization, the ability to measure analyte gases can also be diversified to ethanol, H₂, NH₃, and NO₂. The sensing temperature of the hybrids were varied from room temperature to 280 °C as a function of the amount of insulating metal oxides. As for the sensing mechanism of the TMDs hybrids, the metal oxide nanocrystals generally served as the major gas adsorption centers and the 2D TMDs likely act as conductance channels with semiconducting behavior. Meanwhile, the charge carrier depletion layer or an energy barrier created at heterojunctions may offer extra reaction sites. To comprehend the improved performance of the hybridization, the junction effect should be highlighted. Several examples of hybrids and the proposed mechanisms for the collective effects will be elaborated in the following sections. Since the synergistic effect and gas sensing performance of the hybrids are ineluctably

Table 4. Literature of Gas Sensing Conditions of TMD/Metal Oxide Hybrids and Their Sensing Performances

TMD	MO	synthesis process	morphology of MO	working temp (°C)	analyte	concentration	gas response, $\Delta R/R_a$ (%)	limit of detection	effect	dominant sensing parts	ref
MoS ₂	SnO ₂	hydrothermal	NPs	280	ethanol	200 ppm	120 ^a	50 ppm	operable temperature↓ gas response↑ selectivity↑	MO/p-n junction	74
		hydrothermal	nanofibers	230	TEA	100 ppm	24.9 ^a	5 ppm	operable temperature↓ gas response↑ selectivity↑ stability↑	MO/p-n junction	75
		thermal treatment	NPs	RT	NO ₂	10 ppm	28	0.5 ppm	stability↑ gas response↑ selectivity↑ recovery time↓	MoS ₂ /n-n junction	76
ZnO	layer-by-layer		nanorods	RT	NH ₃	100 ppm	61.92	12 ppb	gas response↑	MO/n-n junction	77
	two-step hydrothermal		NPs	260	ethanol	50 ppm	42.8 ^a	50 ppm	gas response↑ selectivity↑	MO	78
TiO ₂	hydrothermal		nanotubes	150 °C	ethanol	100 ppm	14.2 ^a	50 ppm	gas response↑	MoS ₂ /p-n junction	79
Co ₃ O ₄	layer-by-layer		nanorods	RT	NH ₃	0.1 ppm	10.3	0.1 ppm	gas response↑ selectivity↑ response and recovery time↓	MO/p-n junction	80
WS ₂	TiO ₂	vacuum filtering	quantum dots	RT	NH ₃	500 ppm	56.69	20 ppm	gas response↑ selectivity↑ response and recovery time↓ stability↑	MO/p-n junction	81
WO ₃	annealing		flat shape	150	H ₂ NH ₃ NO ₂	10 ppm	2.9 4.9	1 ppm 1 ppm 100 ppb	stability↑	WS ₂	82
	mix		NPs	25–250	NH ₃	2000 ppm	12.6 ^b	250 ppm	operable temperature↓ gas response↑ selectivity↑	MO/n-n junction	83
SnS ₂	SnO ₂	oxidizing	NPs	80	NO ₂	8 ppm	5.3 ^a	1 ppm	gas response↑ response and recovery time↓	SnS ₂ /n-n junction	84
		microwave/thermal oxidation	NPs	100	NO ₂	1 ppm	51.1 ^a	125 ppb	gas response↑ selectivity↑	SnS ₂ /MO/n-n junction	66
		thermal oxidation	NPs	RT	NH ₃	10 ppm	1.16	10 ppm	gas response↑	MO/n-n junction	85
		hydrothermal sulfuration	nanotubes	RT	NH ₃	100 ppm	2.48 ^c	1 ppm	gas response↑	n-n junction	86

^aR_a/R_g. ^b250 °C. ^cI_g/I_a. Abbreviations: MO, metal oxide; NPs, nanoparticles; RT, room temperature.

influenced by the choice of material with their innate semiconducting properties, we have classified this section by the hybrid type.

MoS₂ + Metal Oxide Hybrids. SnO₂ is possibly the most studied n-type semiconductor for gas sensing applications, and the attempts to integrate SnO₂ with MoS₂ can be a logical pathway. Yan et al.⁷⁴ reported that dispersing SnO₂ nanoparticles on MoS₂ nanosheets (SnO₂@MoS₂) improved the gas sensing performance to ethanol. Figure 6a

shows the field emission scanning electron microscopes (FESEM) image of SnO₂@MoS₂ hybrids where overlapped MoS₂ nanosheets created a 3D flower-like structure. In comparison to pure SnO₂, the operating temperature of the SnO₂@MoS₂ hybrids became lowered, but the higher response value was obtained. The highest gas response was attained at 280 °C for the hybrids while that of pure SnO₂ was at 340 °C (Figure 6b). In addition, the selectivity to ethanol was also

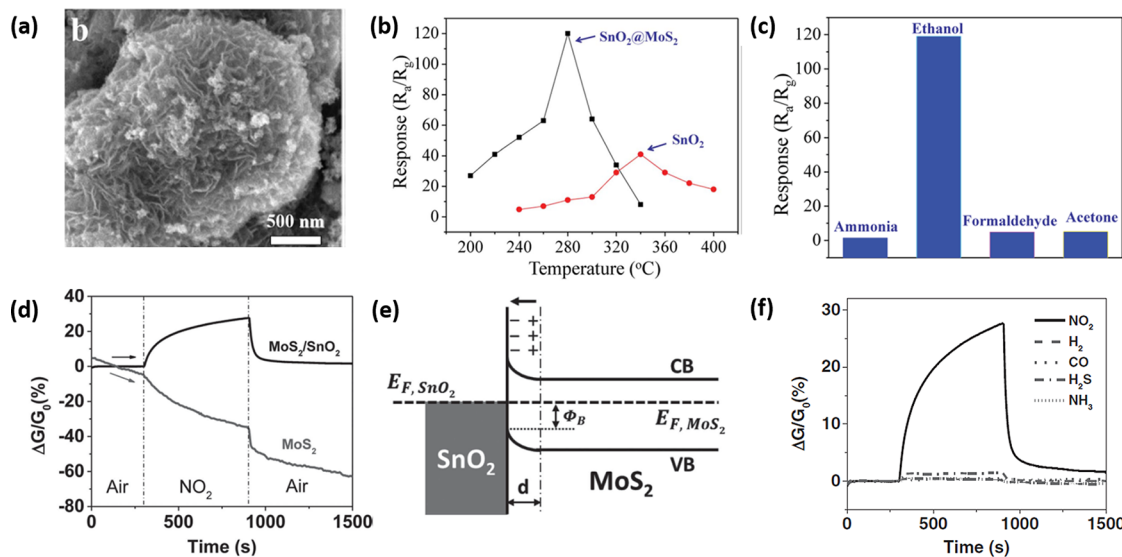


Figure 6. (a) FESEM image of $\text{SnO}_2@\text{MoS}_2$ composites. (b) Correlation between gas response to 200 ppm ethanol and the operating temperature for the sensors based on $\text{SnO}_2@\text{MoS}_2$ composites, and pure SnO_2 nanoparticles. (c) Response of the sensor based on $\text{SnO}_2@\text{MoS}_2$ composites to various test gases. (d) The room temperature dynamic sensing response of MoS_2 nanosheets with and without SnO_2 nanocrystal decoration to 10 ppm of NO_2 in a dry air environment, indicating the SnO_2 nanocrystals significantly enhanced the stability of MoS_2 in the dry air. (e) Band diagram of the $\text{MoS}_2/\text{SnO}_2$ nanohybrid. The E_{F,SnO_2} and E_{F,MoS_2} are Fermi levels of SnO_2 and MoS_2 , respectively. The CB and VB are the conductance and valence band edges of MoS_2 , respectively. d is the thickness of the electron depletion zone, and Φ_B is the Schottky barrier height. (f) Sensing response of the $\text{MoS}_2/\text{SnO}_2$ nanohybrid to various gases at a concentration of 10 ppm.

highly improved through the hybridization (Figure 6c). It is reasonable to assume that the enhanced sensing performances result from the collective geometrical and electronic effects. The increased surface area of MoS_2 layers by inserted SnO_2 nanoparticles offers more active sites for better facilitation of ethanol diffusion and faster electron transfer. In addition, the p-n junction at the interface of SnO_2 (n-type) and MoS_2 (p-type) also forms a built-in internal electric field, which accelerates the electron transfer. The tuned heterojunctions of MoS_2 and SnO_2 was also reported by Qiao et al.⁷⁵ for the efficient gas sensor. In their work, MoS_2 (n-type)/ SnO_2 (p-type) heterojunctions were tailored as a function of MoS_2 loading, and this hierarchical p-n heterojunction exhibit great potential for both gas sensor and catalysts. With a small amount of MoS_2 (molar ratio of Mo/Sn = 0.53), the p-n junction showed superior sensing selectivity and long-term stability to trimethylamine (TEA) at 230 °C. Such superior sensing performance of the hybridized sensor based on TMDs and metal oxide was also commonly observed at low temperature. Cui et al.⁷⁶ decorated SnO_2 nanocrystals onto MoS_2 nanosheets by a wet chemistry method followed by an annealing process and reported an interesting hybridization effect on sensing performance at room temperature. The octahedral phase (1T- MoS_2) with metallic properties was transformed to trigonal prismatic MoS_2 (2H- MoS_2) with semiconducting properties after annealing at 300 °C for 1 h. The combination of the pristine 2H- MoS_2 with n-type semiconducting properties and absorbed oxygen acting as p-type dopant resulted in bipolar characteristics after hybridization. The gas sensing behavior of the SnO_2 decorated - MoS_2 was surprisingly converted to p-type toward NO_2 gas, while both SnO_2 and MoS_2 showed n-type behavior (Figure 6d). The reasons for the phenomena are unclear. However, the authors believed that the SnO_2 nanoparticles served as strong p-type dopants to the MoS_2 nanosheets, which induces dominant p-type behavior of the nanohybrid. Their proposed sensing mechanism predicts that SnO_2 nanocrystals likely served as the major gas adsorption centers and MoS_2 acted as the conductance channels at room temperature. Intimate electrical contact between two dissimilar semiconducting materials usually results in charge transfer and the formation of a charge depletion layer. Since the work function of the SnO_2 (5.7 eV) is larger than that of MoS_2 (5.2 eV), electrons are transferred from MoS_2 to SnO_2 . This transfer creates depletion layers and a Schottky barrier (Figure 6e). The created depletion layers at the interface can prolong the stability and improve

selectivity of the hybrid sensor (Figure 6f). Because the electron depletion zone acts as a passivation layer, the impeded interaction between atmospheric oxygen and MoS_2 increases the long-term stability of the SnO_2 -decorated MoS_2 nanohybrids. This explanation was validated by the experimental results that show extended stability with increasing the amounts of SnO_2 loaded. In addition, the improved selectivity to NO_2 can be ascribed to the incorporation of SnO_2 because the pristine MoS_2 was sensitive to both NO_2 and NH_3 .^{87,88} However, the mechanism on the selective response of SnO_2 to NH_3 remains to be investigated.

ZnO is another n-type semiconductor with a wide band gap of 3.37 eV. ZnO has been intensively investigated as a sensing material along with SnO_2 . The gas sensing characteristics of MoS_2 and ZnO hybrids were explored by Zhang et al.⁷⁷ A multilayered film of MoS_2/ZnO was prepared via a layer-by-layer self-assembly technique with poly(diallyldimethylammonium chloride) (PDDA)/poly(sodium 4-styrenesulfonate) (PSS) as precursor layers (Figure 7a). Gas sensing properties of MoS_2/ZnO , MoS_2/PDDA and a pure ZnO sensor were comparatively studied. During ammonia sensing, the MoS_2/ZnO hybrid presented n-type sensing behavior at room temperature. The higher gas response was observed from the MoS_2/ZnO sensor in comparison with MoS_2/PDDA or pure ZnO sensor (Figure 7b). For example, the normalized gas response values to 5 ppm ammonia are 23.96%, 19.63% and 5.97% for the MoS_2/ZnO , MoS_2/PDDA , and pure ZnO sensors in order. In addition, the fast response and recovery time of the MoS_2/ZnO sensor were measured to be 10 and 11 s under 50 ppm ammonia. The enhanced gas sensing performance was explained based on the synergistic effects of both MoS_2 and ZnO . When oxygen is absorbed on the ZnO surface mainly in the form of O_2^- at room temperature, the oxygen ion acts as an electron acceptor and captures electrons from the conduction band of the sensing material. The absorbed oxygen ions react with gas molecules and transfer electrons to the conduction band of ZnO and MoS_2/ZnO interface. An energy barrier ($\Delta E_B = W_{\text{ZnO}} - W_{\text{MoS}_2}$) can be created at the interface of MoS_2 and ZnO where $W_{\text{ZnO}} = 4.43$ eV and $W_{\text{MoS}_2} = 4.33$ eV. Figure 7c illustrates the band structure of MoS_2/ZnO upon the creation of a heterojunction at the interface after equilibrating the Fermi energy level. Due to aforementioned transferred electrons, the Fermi level of ZnO shifts toward the conduction band, and the energy barrier height at the interface of MoS_2/ZnO is reduced. As a result, the resistance of the

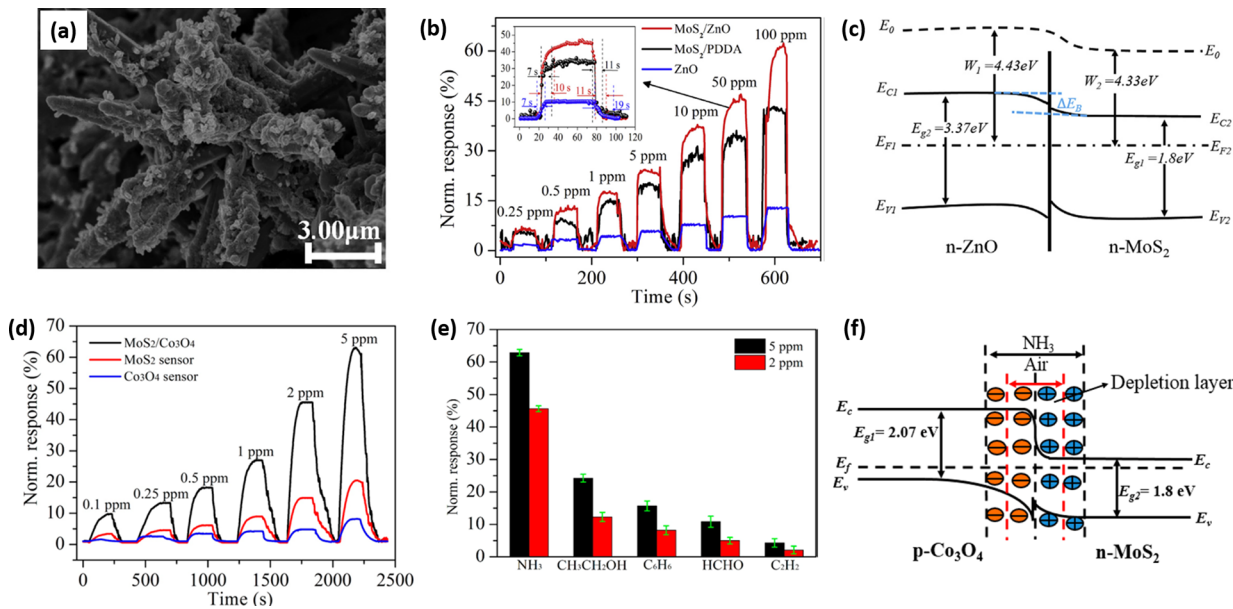


Figure 7. (a) SEM characterization of MoS₂/ZnO nanocomposite (b) Normalized responses of MoS₂/ZnO, MoS₂/PDDA and ZnO film sensors exposed to various ammonia gas concentrations at room temperature, and the inset indicates the response and recovery characteristics of these sensors exposed to 50 ppm ammonia gas. (c) Schematic illustration of the energy-band structure of the sensor (E_0 is vacuum-energy level, W is work function, E_g is energy band gap, E_F is Fermi-energy level, E_C is the conduction band, and E_V is the valence band). (d) Normalized response of the MoS₂/Co₃O₄, MoS₂, and Co₃O₄ film sensors toward various ammonia concentrations. (e) Selectivity of the MoS₂/Co₃O₄ film sensor upon exposure to ammonia (NH₃), ethanol (CH₃CH₂OH), benzene (C₆H₆), formaldehyde (HCHO), and acetylene (C₂H₂) with concentrations of 5 and 2 ppm, respectively. (f) Energy band structure diagram and resistance variation for the n-type MoS₂/p-type Co₃O₄ hybrid in air and ammonia.

MoS₂/ZnO hybrid sensors decreases. Along with the n-n junction effect, a higher specific surface area of the hybrid structure can provide higher quantities of efficient electron pathways and active centers of gas absorption.

In contrast to n-type semiconducting oxides, Zhang et al.⁸⁰ hybridized a p-type semiconductor cobalt oxide (Co₃O₄) with MoS₂ to investigate the function of opposite majority carriers in the hybrid. The MoS₂/Co₃O₄ hybrid film with five self-assembled layers yielded the highest gas response among the one, three, five, and seven layers, probably due to a good balance between conductivity of the sensor and gas diffusion between layers. The fabricated p-n-type hybrids showed p-type sensing behavior toward ammonia (Figure 7d). In addition, the selectivity of the MoS₂/Co₃O₄ hybrid toward ammonia was superior to ethanol (CH₃CH₂OH), benzene (C₆H₆), formaldehyde (HCHO), and acetylene (C₂H₂) (Figure 7e). In this hybrid, Co₃O₄ serves as an electron acceptor, creating a hole accumulation layer (HAL). Under ammonia exposure, the gas molecules react with adsorbed oxygen ions (O_{ads}²⁻) by releasing electrons from ammonia, resulting in the decreased HAL width and increased resistance of the hybrid. It is believed that the results of the MoS₂/Co₃O₄ hybrid can provide convincing evidence on the junction effects in sensing mechanisms of TMD-MO system. MoS₂ is an n-type semiconductor with 1.2–1.9 eV band gap while Co₃O₄ is a p-type semiconductor with 2.07 eV band gap. With their contact, the interdiffusion of each majority carrier drives to form a depletion layer at the interface (p-n junction). The holes in Co₃O₄ and electrons in MoS₂ create a self-built electric field and establish a depletion layer at the p-n junction that is equilibrating with the Fermi level. The depletion layer can be modulated as a function of adsorption and desorption of the gas molecules. Figure 7f depicts the variation of the width of the depletion layer upon exposure to air and ammonia gas. With ammonia injection, free electrons were released from ammonia through the interaction between O_{ads}²⁻, and neutralized the holes in the Co₃O₄. Accordingly, it contributes to the expansion of the depletion layer, which increases the resistance of the hybrid sensor. Such combination of the junction effect along with the electrical and structural benefits from its layered structure can offer an understanding of superior sensing performance of the MoS₂/Co₃O₄ hybrid.

WS₂ + Metal Oxide Hybrids. TiO₂ is a well-known wide band gap n-type semiconductor with good thermal and chemical stability. The

sensing properties of TiO₂ quantum dot (QD) decorated 2D WS₂ were demonstrated by Qin et al.⁸¹ Chemically exfoliated 2D WS₂ nanosheets were hybridized with TiO₂ QDs (3–4 nm) under different ratios from 0.44 to 1.65 of TiO₂/WS₂ by vacuum filtering. The gas response to ammonia was highest with 0.44 TiO₂/WS₂ ratio and decreased with further increasing TiO₂ amount (Figure 8a). Excessive TiO₂ QDs coverage appears to degrade the electrical conduction in addition to the difficult interaction between the ammonia gas and the hybrid. The hybridized TiO₂/WS₂ sensors had higher gas response and selectivity, with shorter recovery time and improved stability compared to bare WS₂ monolayer-based sensors. Figure 8b presents nearly 17 times higher response of the TiO₂/WS₂ hybrid than the bare WS₂ with improved selectivity to ammonia, as shown in Figure 8c. After combining two materials, the electrons in the conduction band of WS₂ were transferred to that of TiO₂, followed by the creation of a large depletion region at the interface between TiO₂ QDs and WS₂, as illustrated in Figure 8d. The improved gas response of the hybrid can be ascribed to the expansion of depletion layers and the numbers of reaction active sites by TiO₂ QDs. Limited improvement of sensing performance in the large size of TiO₂ for the hybrids implies that the size of the metal oxide should be carefully chosen. Interestingly, the hybrids showed improved stability on gas sensing under ambient conditions. It is reported that absorption of oxygen from atmosphere onto the surface of 2D materials induces to the negative shift of the base current of the WS₂ sensor at room temperature, influencing on long-term stability.⁸⁹ In the hybrids, the presence of the depletion region on the interface would reduce the interaction between WS₂ and ambient oxygen gas. The depletion region could function as passivation layers, resulting in significantly extended stability of the hybrids.

SnS₂ + Metal Oxide Hybrids. SnO₂ can be an excellent material to be grafted to SnS₂ because the simple physical mixing between SnO₂ and SnS₂ in this hybrid can leverage to the composition-tunable band gap. Besides the heterojunction effect, the SnS₂/SnO₂ hybrids have demonstrated to create a hierarchical structure for better geometrical effects. Flower-like hierarchical SnS₂/SnO₂ hybrids were fabricated by a microwave method and thermal oxidation by Hao et al.⁶⁶ The average size of the flower-like SnS₂/SnO₂ nanohybrids is around 1 μm diameter, with a uniform distribution of ultrafine SnO₂ nanoparticles (Figure 9a).

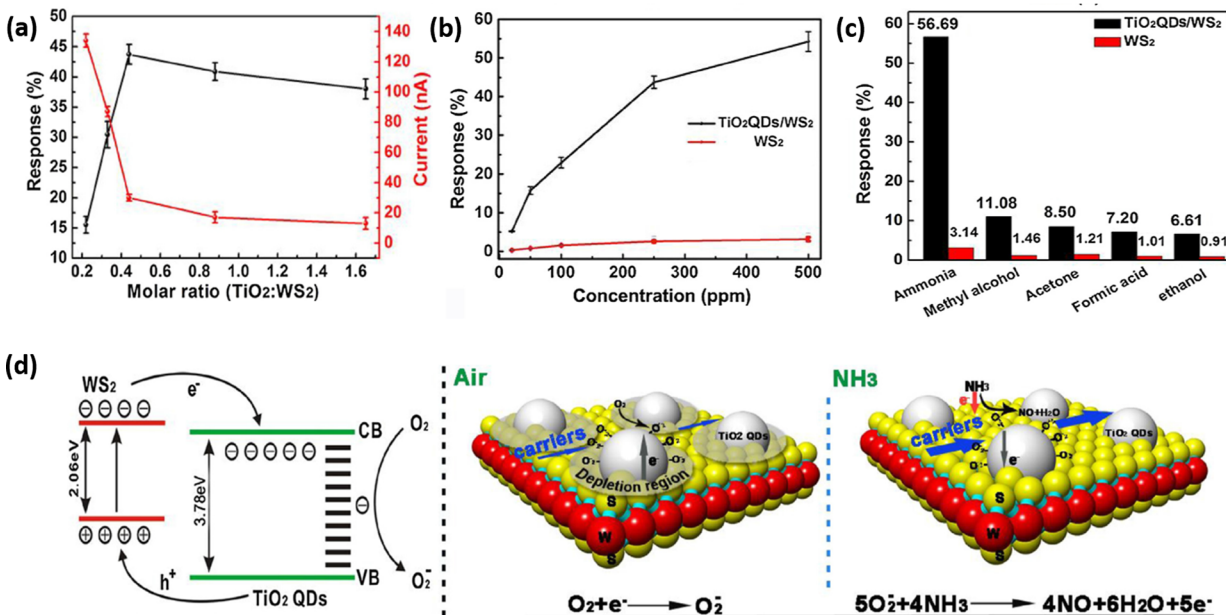


Figure 8. (a) Response of TiO_2 QDs/ WS_2 nanohybrids and the current baseline as a function of different molar ratios (0.22, 0.33, 0.44, 0.88, 1.65) upon exposure to 250 ppm of NH_3 . (b) The response of gas sensors based on 0.44 TiO_2 QDs/ WS_2 nanohybrids, large particle TiO_2 / WS_2 and monolayer WS_2 as a function of different concentrations of ammonia gas from 20 to 500 ppm. (c) Selectivity of the sensors based on the 0.44 TiO_2 QDs/ WS_2 nanohybrids and monolayer WS_2 upon exposure to 500 ppm of various gases. (d) Energy band diagram of the TiO_2 / WS_2 nanohybrids and the schematic of the interfacial interaction between the TiO_2 / WS_2 nanohybrids structure and NH_3 molecules.

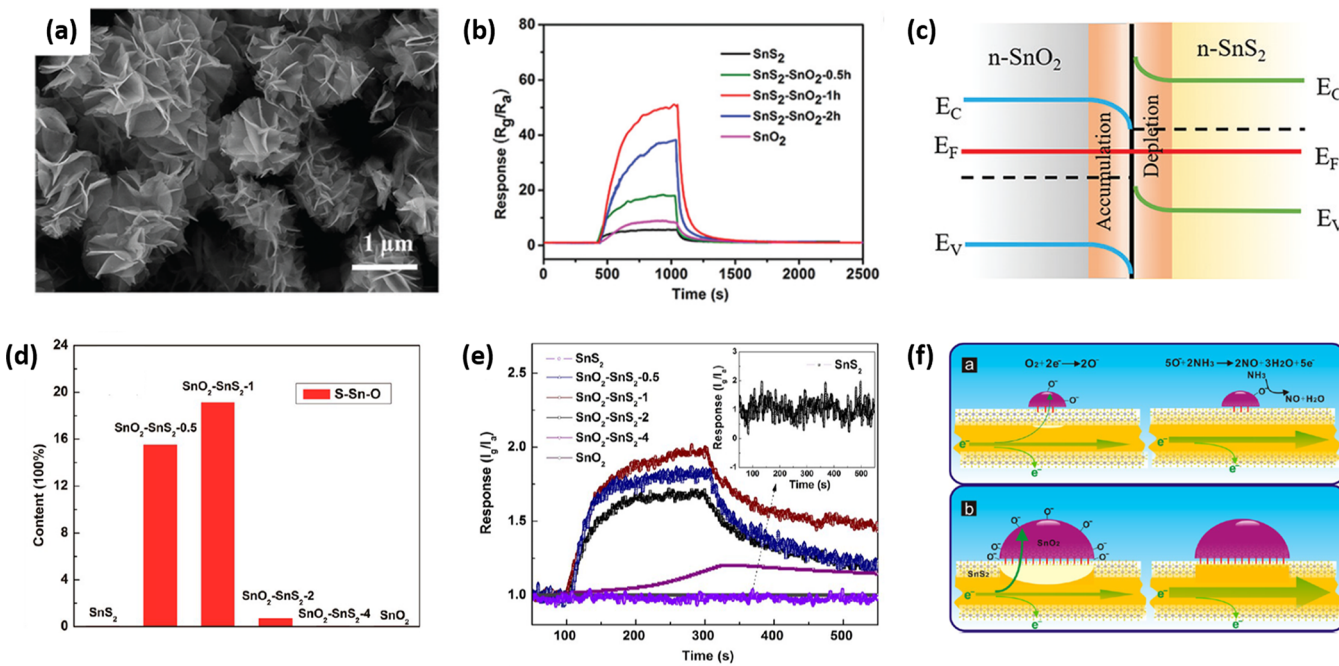


Figure 9. (a) SEM image of the fabrication of SnS_2 / SnO_2 nanocomposites. (b) Response curves of the sensors based on pure SnS_2 , SnS_2 - SnO_2 , and pure SnO_2 with different oxidation times toward 1 ppm of NO_2 at an operating temperature of 100 $^\circ\text{C}$. (c) Band structure model of the SnS_2 / SnO_2 heterojunctions. E_F is the Fermi level, and E_C and E_V are the conductance and valence bands, respectively. (d) Semiquantitative analysis of the fraction of O-Sn-S among the total of O-Sn-O, O-Sn-S, and O-Sn. (e) Dynamic response-recovery curves of the obtained samples to 100 ppm of NH_3 at room temperature. The inset shows a larger version of SnS_2 . (f) Schematic of the SnO_2 - SnS_2 hybrid with [a] a small amount and [b] a large amount of chemical bonds at the interface and their corresponding gas-sensing process.

All SnS_2 , SnO_2 , and SnS_2 / SnO_2 hybrids showed n-type sensing behavior to NO_2 gas. From the experiment to form SnO_2 on SnS_2 by partial oxidation, the gas response was enhanced with increasing oxidation time, and then the response declined after 1 h oxidation. The initial increase can be attributed to the facilitated adsorption of NO_2 by the formed SnO_2 nanoparticles. Excessive oxidation to fully oxidize

SnS_2 nanosheets degraded the sensing response (Figure 9b). The sensing mechanism of SnS_2 / SnO_2 nanohybrids can be understood in terms of two factors: heterojunction and hybridized nanostructure (Figure 9c). Electronically, the n-n junction is constructed between SnS_2 nanosheets and SnO_2 nanoparticles. With band bending, an accumulation layer is built on the SnO_2 side, and a depletion layer is

formed on the SnS_2 side. Under oxygen presence, the accumulation layer can be shrunk by oxygen absorption followed by the formation of O_2^- by taking electrons from the layer. Such an accumulation layer results in the decreased resistance and increased charge transfer during the sensing process. In contrast, the NO_2 gas molecules react with O_2^- by withdrawing electrons from SnO_2 . Then more electrons are transferred from SnS_2 to SnO_2 until a new equilibrium is achieved, leading to a widened depletion layer and increased resistance. As a result, it is evident that the number of n-n junctions significantly influences the sensing response. Structurally, the large space between SnS_2 nanosheets in the hierarchical structure via dispersed SnO_2 is beneficial for the gas molecules diffusion. Chemically, the bonds of S–Sn–O created between SnS_2 and SnO_2 act as an efficient charge transport bridge during gas sensing process. The chemical effects were supported by similar experiments of SnO_2 – SnS_2 hybrids by thermal oxidation of SnS_2 at 300 °C.⁸⁵ XPS results confirmed that the peak intensity of interfacial bonds increased due to the increased amount of interfacial bonds between SnO_2 and SnS_2 , and then it decreased after 1 h of oxidation (Figure 9d). The highest response to ammonia was attained from the SnO_2 – SnS_2 hybrid sample oxidized for 1 h (Figure 9e). It is apparent that the interfacial bond of SnO_2 and SnS_2 is closely related to the sensing mechanism. At the interface, the charge carriers can be trapped due to dangling bonds, and an additional depletion layer can be formed at the interface. Equation 7 explains the density of chemisorbed oxygen on the surface of SnO_2 governs the gas sensing properties of the SnO_2 – SnS_2 hybrids.

$$3Q_2 = r_2 N_{d1} \exp\left(-\frac{eQ_i^2}{2\varepsilon k T N_{d1}}\right) \quad (7)$$

where Q_2 is the density of chemisorbed oxygen on the surface of SnO_2 , r_2 is the radius of SnO_2 hemispheres, N_{d1} is the donor density of SnS_2 , Q_i is the density of chemisorbed oxygen on the interface state density, ε is the dielectric constant of SnS_2 , k is Boltzmann constant, T is temperature. With a small number of interfacial bonds, few electrons are able to pass across the depletion layer because of the high energy barrier. According to eq 7, a small amount of chemisorbed oxygen can be generated, which results in a low gas response. On the other hand, the density of chemisorbed oxygen can be enlarged with the formation of interfacial bonds for the enhanced gas performance (Figure 9f). Therefore, various parameters associated with hybridization should be considered to predict the overall gas response.

CONCLUSIONS AND OUTLOOK

In this Review, we comprehensively compiled achievements in recent research on 2D TMDs and metal oxide hybrids. The structure and basic characteristics of newly emerged 2D TMDs were introduced with a brief explanation on the sensing mechanisms of metal oxide and 2D TMDs. Their synthesis methods and distinctive gas sensing properties were subsequently summarized. To improve and refine the sensing performance of 2D TMDs, the integration of 2D TMDs with metal oxides was explored. The collective benefits and mechanisms of TMDs and metal oxides were discussed in three aspects: geometrical effects, electronic effects, and chemical effects. Some results showed promising performances such as high sensitivity and selectivity to analyte gases even at room temperature. Such achievements offer great potential for practical implementation as gas sensors.

Although significant progress has been demonstrated, there are still remaining questions to understand the underlying mechanisms to develop devices for real-life applications. First, a clear understanding of the synergistic or hybridized effects in 2D TMD and metal oxide hybrids should be determined. The geometrical effects of hybridization have been often described, but the electronic and chemical effects have not been clearly explained. Throughout relevant research papers, there are various electronic and chemical explanations for the improved

gas sensing performance. However, there is no clear answer as to which electrical modification corresponds to each specific performance improvement. Most references only addressed the charge carrier flow based on the Fermi energy difference and the formation of depletion layers regardless of the type of heterostructure. The relationship between the modified properties and the enhanced performance should be more clearly defined in terms of electronic or chemical mechanisms. In addition, little work has been done to address a thorough scientific comprehension of enhanced selectivity due to the heterostructures. Several references mentioned improved selectivity through hybridization, but such improvement has not been clearly explained. More simulated or experimental results can clarify this vague explanation. Second, a rational justification of the hybrid design is required in terms of material selection. When designing a hybrid, a researcher should consider the Fermi energy and work functions of each material, as well as the dominant sensing material. The direction of the charge carrier transfer at the interface and the dominant sensing material will be critical in the sensing mechanism and the sensing performance. Unclear information of the contact type, either Schottky or ohmic, at the heterojunction limits the ability to determine which contact is more favorable to improve the gas sensing performance. Further study should be focused on this aspect.

In terms of future prospectives, there are tremendous opportunities to investigate 2D TMD materials and their boundless combinations with metal oxides for sensor applications. Going forward, new materials, and their hybrids, with innovative designs will be a promising option. Compared to graphene-based gas sensors, little attention has been paid to 2D TMD sensors. In addition, the functionalization of TMDs though metal oxide hybridizations is still at an early stage of research. In the case of MoSe_2 and MoTe_2 for sensor applications, no results have been published on their possible metal oxide hybrids. In this regard, simulation results could guide the insight for a heterostructure design prior to an experimental investigation. In addition, an investigation on surface treatment can elucidate the sensing mechanisms and garnish sensing performance for further advancement. Previous studies have examined the surface treatment of 2D nanomaterials, using techniques such as UV treatment or thermal annealing. By introducing photo-reactive materials into the heterostructure, the performances on gas response and the response/recovery time can be improved in addition to gaining knowledge on photoinduced charger transfer. For instance, it has been reported that the perovskite crystal structure shows great photoreactivity.^{90,91} By decorating perovskite structured metal oxides on 2D TMDs, photo-activated effects can be magnified, resulting in boosted performance.

AUTHOR INFORMATION

Corresponding Authors

*E-mail: dkim@auburn.edu. Tel.: 1-334-844-4864. Fax: 1-334-844-3400.

*E-mail: benedicto@gachon.ac.kr. Tel.: 82-011-9766-5558.

ORCID

Eunji Lee: 0000-0001-5046-3060

Dong-Joo Kim: 0000-0001-5013-4005

Notes

The authors declare no competing financial interest.

ACKNOWLEDGMENTS

This research was partially supported by the Korea Institute of Energy Technology Evaluation and Planning (KETEP), by a grant funded by the Korea Government Ministry of Trade, Industry and Energy (20158520000210), and by the Agency for Defense Development (ADD) as global cooperative research for high performance and lightweight biourine-based fuel cell (UD160050BD). The authors deeply appreciate Benjamin Keith for his valuable efforts on this manuscript.

VOCABULARY

gas response, a change of measured signal per analyte concentration unit; selectivity, the ability of gas sensors to identify a specific gas among a gas mixture (response of target/R of interference); stability, the ability of a sensor to provide reproducible results for a certain period of time; heterojunction, the interface that occurs between two layers of dissimilar crystalline semiconductors; Fermi energy, the highest energy that the electrons assume at $T = 0\text{ K}$.

REFERENCES

- (1) Zhang, X.; Hou, L.; Ciesielski, A.; Samori, P. 2d Materials Beyond Graphene for High-Performance Energy Storage Applications. *Adv. Energy Mater.* **2016**, *6*, 1600671.
- (2) Shao, Y.; Wang, J.; Wu, H.; Liu, J.; Aksay, I. A.; Lin, Y. Graphene Based Electrochemical Sensors and Biosensors: A Review. *Electroanalysis* **2010**, *22*, 1027–1036.
- (3) Liu, X.; Ma, T.; Pinna, N.; Zhang, J. Two-Dimensional Nanostructured Materials for Gas Sensing. *Adv. Funct. Mater.* **2017**, *27*, 1702168.
- (4) Garcia, J. C.; de Lima, D. B.; Assali, L. V.; Justo, J. F. Group Iv Graphene-and Graphane-Like Nanosheets. *J. Phys. Chem. C* **2011**, *115*, 13242–13246.
- (5) Yang, W.; Gan, L.; Li, H.; Zhai, T. Two-Dimensional Layered Nanomaterials for Gas-Sensing Applications. *Inorg. Chem. Front.* **2016**, *3*, 433–451.
- (6) Barzegar, M.; Tudu, B. Two-Dimensional Materials for Gas Sensors: From First Discovery to Future Possibilities. *Surf. Innovations* **2018**, *6*, 205–230.
- (7) Tricoli, A.; Nasiri, N.; De, S. Wearable and Miniaturized Sensor Technologies for Personalized and Preventive Medicine. *Adv. Funct. Mater.* **2017**, *27*, 1605271.
- (8) Schedin, F.; Geim, A.; Morozov, S.; Hill, E.; Blake, P.; Katsnelson, M.; Novoselov, K. Detection of Individual Gas Molecules Adsorbed on Graphene. *Nat. Mater.* **2007**, *6*, 652.
- (9) Late, D. J.; Huang, Y.-K.; Liu, B.; Acharya, J.; Shirodkar, S. N.; Luo, J.; Yan, A.; Charles, D.; Waghmare, U. V.; Dravid, V. P.; Rao, C. N. R. Sensing Behavior of Atomically Thin-Layered MoS₂ Transistors. *ACS Nano* **2013**, *7*, 4879–4891.
- (10) Abbas, A. N.; Liu, B.; Chen, L.; Ma, Y.; Cong, S.; Aroonyadet, N.; Köpf, M.; Nilges, T.; Zhou, C. Black Phosphorus Gas Sensors. *ACS Nano* **2015**, *9*, 5618–5624.
- (11) Lee, E.; VahidMohammadi, A.; Prorok, B. C.; Yoon, Y. S.; Beidaghi, M.; Kim, D.-J. Room Temperature Gas Sensing of Two-Dimensional Titanium Carbide (Mxene). *ACS Appl. Mater. Interfaces* **2017**, *9*, 37184–37190.
- (12) Cho, S. Y.; Lee, Y.; Koh, H. J.; Jung, H.; Kim, J. S.; Yoo, H. W.; Kim, J.; Jung, H. T. Superior Chemical Sensing Performance of Black Phosphorus: Comparison with MoS₂ and Graphene. *Adv. Mater.* **2016**, *28*, 7020–7028.
- (13) Park, W.; Park, J.; Jang, J.; Lee, H.; Jeong, H.; Cho, K.; Hong, S.; Lee, T. Oxygen Environmental and Passivation Effects on Molybdenum Disulfide Field Effect Transistors. *Nanotechnology* **2013**, *24*, 095202.
- (14) Kim, T. H.; Kim, Y. H.; Park, S. Y.; Kim, S. Y.; Jang, H. W. Two-Dimensional Transition Metal Disulfides for Chemoresistive Gas Sensing: Perspective and Challenges. *Chemosensors* **2017**, *5*, 15.
- (15) Choi, W.; Choudhary, N.; Han, G. H.; Park, J.; Akinwande, D.; Lee, Y. H. Recent Development of Two-Dimensional Transition Metal Dichalcogenides and Their Applications. *Mater. Today* **2017**, *20*, 116–130.
- (16) Yang, S.; Jiang, C.; Wei, S.-h. Gas Sensing in 2d Materials. *Appl. Phys. Rev.* **2017**, *4*, 021304.
- (17) Choi, S.-J.; Kim, I.-D. Recent Developments in 2d Nanomaterials for Chemiresistive-Type Gas Sensors. *Electron. Mater. Lett.* **2018**, *14*, 221–260.
- (18) Neri, G. Thin 2d: The New Dimensionality in Gas Sensing. *Chemosensors* **2017**, *5*, 21.
- (19) Varghese, S. S.; Varghese, S. H.; Swaminathan, S.; Singh, K. K.; Mittal, V. Two-Dimensional Materials for Sensing: Graphene and Beyond. *Electronics* **2015**, *4*, 651–687.
- (20) Choopun, S.; Hongsth, N.; Wongrat, E. Metal-Oxide Nanowires for Gas Sensors. *InTech* **2012**, DOI: [10.5772/54385](https://doi.org/10.5772/54385).
- (21) Wang, C.; Yin, L.; Zhang, L.; Xiang, D.; Gao, R. Metal Oxide Gas Sensors: Sensitivity and Influencing Factors. *Sensors* **2010**, *10*, 2088–2106.
- (22) Miller, D. R.; Akbar, S. A.; Morris, P. A. Nanoscale Metal Oxide-Based Heterojunctions for Gas Sensing: A Review. *Sens. Actuators, B* **2014**, *204*, 250–272.
- (23) Radisavljevic, B.; Radenovic, A.; Brivio, J.; Giacometti, i. V.; Kis, A. Single-Layer MoS₂ Transistors. *Nat. Nanotechnol.* **2011**, *6*, 147–150.
- (24) Andoshe, D. M.; Jeon, J.-M.; Kim, S. Y.; Jang, H. W. Two-Dimensional Transition Metal Dichalcogenide Nanomaterials for Solar Water Splitting. *Electron. Mater. Lett.* **2015**, *11*, 323–335.
- (25) Das, S.; Chen, H.-Y.; Penumatcha, A. V.; Appenzeller, J. High Performance Multilayer MoS₂ Transistors with Scandium Contacts. *Nano Lett.* **2013**, *13*, 100–105.
- (26) Castellanos-Gomez, A.; Poot, M.; Steele, G. A.; van der Zant, H. S.; Agrait, N.; Rubio-Bollinger, G. Elastic Properties of Freely Suspended MoS₂ Nanosheets. *Adv. Mater.* **2012**, *24*, 772–775.
- (27) Zeng, H.; Dai, J.; Yao, W.; Xiao, D.; Cui, X. Valley Polarization in MoS₂ Monolayers by Optical Pumping. *Nat. Nanotechnol.* **2012**, *7*, 490–493.
- (28) Ganatra, R.; Zhang, Q. Few-Layer MoS₂: A Promising Layered Semiconductor. *ACS Nano* **2014**, *8*, 4074–4099.
- (29) Sik Hwang, W.; Remskar, M.; Yan, R.; Protasenko, V.; Tahy, K.; Doo Chae, S.; Zhao, P.; Konar, A.; Xing, H.; Seabaugh, A.; Jena, D. Transistors with Chemically Synthesized Layered Semiconductor Ws₂ Exhibiting 105 Room Temperature Modulation and Ambipolar Behavior. *Appl. Phys. Lett.* **2012**, *101*, 013107.
- (30) Liu, X.; Hu, J.; Yue, C.; Della Fera, N.; Ling, Y.; Mao, Z.; Wei, J. High Performance Field-Effect Transistor Based on Multilayer Tungsten Disulfide. *ACS Nano* **2014**, *8*, 10396–10402.
- (31) Zhao, W.; Ghorannevis, Z.; Chu, L.; Toh, M.; Kloc, C.; Tan, P. H.; Eda, G. Evolution of Electronic Structure in Atomically Thin Sheets of Ws₂ and WSe₂. *ACS Nano* **2013**, *7*, 791–797.
- (32) Late, D. J.; Doneux, T.; Bougouma, M. Single-Layer MoS₂ Based NH₃ Gas Sensor. *Appl. Phys. Lett.* **2014**, *105*, 233103.
- (33) Lu, X.; Utama, M. I. B.; Lin, J.; Gong, X.; Zhang, J.; Zhao, Y.; Pantelides, S. T.; Wang, J.; Dong, Z.; Liu, Z.; et al. Large-Area Synthesis of Monolayer and Few-Layer MoS₂ Films on SiO₂ Substrates. *Nano Lett.* **2014**, *14*, 2419–2425.
- (34) Larentis, S.; Fallahazad, B.; Tutuc, E. Field-Effect Transistors and Intrinsic Mobility in Ultra-Thin MoS₂ Layers. *Appl. Phys. Lett.* **2012**, *101*, 223104.
- (35) Ma, Y.; Dai, Y.; Guo, M.; Niu, C.; Lu, J.; Huang, B. Electronic and Magnetic Properties of Perfect, Vacancy-Doped, and Nonmetal Adsorbed MoS₂, MoSe₂ and WS₂ Monolayers. *Phys. Chem. Chem. Phys.* **2011**, *13*, 15546–15553.
- (36) Umar, A.; Akhtar, M.; Dar, G.; Abaker, M.; Al-Hajry, A.; Baskoutas, S. Visible-Light-Driven Photocatalytic and Chemical Sensing Properties of SnS₂ Nanoflakes. *Talanta* **2013**, *114*, 183–190.
- (37) Ou, J. Z.; Ge, W.; Carey, B.; Daeneke, T.; Rotbart, A.; Shan, W.; Wang, Y.; Fu, Z.; Chrimes, A. F.; Włodarski, W.; et al. Physisorption-

- Based Charge Transfer in Two-Dimensional Sns₂ for Selective and Reversible No₂ Gas Sensing. *ACS Nano* **2015**, *9*, 10313–10323.
- (38) Leenaerts, O.; Partoens, B.; Peeters, F. Adsorption of H₂O, N H₃, Co, N O₂, and No on Graphene: A First-Principles Study. *Phys. Rev. B: Condens. Matter Mater. Phys.* **2008**, *77*, 125416.
- (39) Yue, Q.; Shao, Z.; Chang, S.; Li, J. Adsorption of Gas Molecules on Monolayer Mos₂ and Effect of Applied Electric Field. *Nanoscale Res. Lett.* **2013**, *8*, 425–431.
- (40) Bui, V. Q.; Pham, T.-T.; Le, D. A.; Thi, C. M.; Le, H. M. A First-Principles Investigation of Various Gas (Co, H₂O, No, and O₂) Absorptions on a Ws₂Monolayer: Stability and Electronic Properties. *J. Phys.: Condens. Matter* **2015**, *27*, 305005.
- (41) Feng, Z.; Xie, Y.; Chen, J.; Yu, Y.; Zheng, S.; Zhang, R.; Li, Q.; Chen, X.; Sun, C.; Zhang, H.; et al. Highly Sensitive Mote₂ Chemical Sensor with Fast Recovery Rate through Gate Biasing. *2D Mater.* **2017**, *4*, 025018.
- (42) Cho, B.; Hahm, M. G.; Choi, M.; Yoon, J.; Kim, A. R.; Lee, Y.-J.; Park, S.-G.; Kwon, J.-D.; Kim, C. S.; Song, M.; et al. Charge-Transfer-Based Gas Sensing Using Atomic-Layer Mos₂. *Sci. Rep.* **2015**, *5*, 8052.
- (43) Huang, B.; Li, Z.; Liu, Z.; Zhou, G.; Hao, S.; Wu, J.; Gu, B.-L.; Duan, W. Adsorption of Gas Molecules on Graphene Nanoribbons and Its Implication for Nanoscale Molecule Sensor. *J. Phys. Chem. C* **2008**, *112*, 13442–13446.
- (44) Cho, B.; Kim, A. R.; Park, Y.; Yoon, J.; Lee, Y.-J.; Lee, S.; Yoo, T. J.; Kang, C. G.; Lee, B. H.; Ko, H. C.; et al. Bifunctional Sensing Characteristics of Chemical Vapor Deposition Synthesized Atomic-Layered Mos₂. *ACS Appl. Mater. Interfaces* **2015**, *7*, 2952–2959.
- (45) He, Q.; Zeng, Z.; Yin, Z.; Li, H.; Wu, S.; Huang, X.; Zhang, H. Fabrication of Flexible Mos₂ Thin-Film Transistor Arrays for Practical Gas-Sensing Applications. *Small* **2012**, *8*, 2994–2999.
- (46) Li, H.; Yin, Z.; He, Q.; Li, H.; Huang, X.; Lu, G.; Fam, D. W. H.; Tok, A. I. Y.; Zhang, Q.; Zhang, H. Fabrication of Single-and Multilayer Mos₂ Film-Based Field-Effect Transistors for Sensing No at Room Temperature. *Small* **2012**, *8*, 63–67.
- (47) Xu, T.; Pei, Y.; Liu, Y.; Wu, D.; Shi, Z.; Xu, J.; Tian, Y.; Li, X. High-Response No₂ Resistive Gas Sensor Based on Bilayer Mos₂ Grown by a New Two-Step Chemical Vapor Deposition Method. *J. Alloys Compd.* **2017**, *725*, 253–259.
- (48) Lee, K.; Gatensby, R.; McEvoy, N.; Hallam, T.; Duesberg, G. S. High-Performance Sensors Based on Molybdenum Disulfide Thin Films. *Adv. Mater.* **2013**, *25*, 6699–6702.
- (49) O'Brien, M.; Lee, K.; Morrish, R.; Berner, N. C.; McEvoy, N.; Wolden, C. A.; Duesberg, G. S. Plasma Assisted Synthesis of Ws₂ for Gas Sensing Applications. *Chem. Phys. Lett.* **2014**, *615*, 6–10.
- (50) Li, X.; Li, X.; Li, Z.; Wang, J.; Zhang, J. Ws₂ Nanoflakes Based Selective Ammonia Sensors at Room Temperature. *Sens. Actuators, B* **2017**, *240*, 273–277.
- (51) Qin, Z.; Zeng, D.; Zhang, J.; Wu, C.; Wen, Y.; Shan, B.; Xie, C. Effect of Layer Number on Recovery Rate of Ws₂ Nanosheets for Ammonia Detection at Room Temperature. *Appl. Surf. Sci.* **2017**, *414*, 244–250.
- (52) Xu, T.; Liu, Y.; Pei, Y.; Chen, Y.; Jiang, Z.; Shi, Z.; Xu, J.; Wu, D.; Tian, Y.; Li, X. The Ultra-High No₂ Response of Ultra-Thin Ws₂ Nanosheets Synthesized by Hydrothermal and Calcination Processes. *Sens. Actuators, B* **2018**, *259*, 789–796.
- (53) Qin, Z.; Xu, K.; Yue, H.; Wang, H.; Zhang, J.; Ouyang, C.; Xie, C.; Zeng, D. Enhanced Room-Temperature Nh₃ Gas Sensing by 2d Sns₂ with Sulfur Vacancies Synthesized by Chemical Exfoliation. *Sens. Actuators, B* **2018**, *262*, 771–779.
- (54) Cho, S.-Y.; Kim, S. J.; Lee, Y.; Kim, J.-S.; Jung, W.-B.; Yoo, H.-W.; Kim, J.; Jung, H.-T. Highly Enhanced Gas Adsorption Properties in Vertically Aligned Mos₂ Layers. *ACS Nano* **2015**, *9*, 9314–9321.
- (55) Cha, J.-H.; Choi, S.-J.; Yu, S.; Kim, I.-D. 2d Ws 2-Edge Functionalized Multi-Channel Carbon Nanofibers: Effect of Ws 2 Edge-Abundant Structure on Room Temperature No 2 Sensing. *J. Mater. Chem. A* **2017**, *5*, 8725–8732.
- (56) Huo, N.; Yang, S.; Wei, Z.; Li, S.-S.; Xia, J.-B.; Li, J. Photoresponsive and Gas Sensing Field-Effect Transistors Based on Multilayer Ws 2 Nanoflakes. *Sci. Rep.* **2015**, *4*, 5209.
- (57) Gu, D.; Li, X.; Wang, H.; Li, M.; Xi, Y.; Chen, Y.; Wang, J.; Rumyntseva, M. N.; Gaskov, A. M. Light Enhanced Voc_s Sensing of Ws₂Microflakes Based Chemiresistive Sensors Powered by Triboelectronic Nangenerators. *Sens. Actuators, B* **2018**, *256*, 992–1000.
- (58) Sharma, M.; Jamdagni, P.; Kumar, A.; Ahluwalia, P. Interactions of Gas Molecules with Monolayer Mose₂: A First Principle Study. *AIP Conf. Proc.* **2015**, *140045*.
- (59) Kumar, S.; Kaushik, S.; Pratap, R.; Raghavan, S. Graphene on Paper: A Simple, Low-Cost Chemical Sensing Platform. *ACS Appl. Mater. Interfaces* **2015**, *7*, 2189–2194.
- (60) Liu, B.; Chen, L.; Liu, G.; Abbas, A. N.; Fathi, M.; Zhou, C. High-Performance Chemical Sensing Using Schottky-Contacted Chemical Vapor Deposition Grown Monolayer Mos₂ Transistors. *ACS Nano* **2014**, *8*, 5304–5314.
- (61) Huang, Y.; Sutter, E.; Sadowski, J. T.; Cotlet, M.; Monti, O. L.; Racke, D. A.; Neupane, M. R.; Wickramaratne, D.; Lake, R. K.; Parkinson, B. A.; Sutter, P. Tin Disulfide—an Emerging Layered Metal Dichalcogenide Semiconductor: Materials Properties and Device Characteristics. *ACS Nano* **2014**, *8*, 10743–10755.
- (62) Sun, Y.; Cheng, H.; Gao, S.; Sun, Z.; Liu, Q.; Liu, Q.; Lei, F.; Yao, T.; He, J.; Wei, S.; Xie, Y. Freestanding Tin Disulfide Single-Layers Realizing Efficient Visible-Light Water Splitting. *Angew. Chem., Int. Ed.* **2012**, *51*, 8727–8731.
- (63) Zhao, R.; Wang, T.; Zhao, M.; Xia, C.; Zhao, X.; An, Y.; Dai, X. A Theoretical Simulation of Small-Molecules Sensing on an S-Vacancy Sns₂ Monolayer. *Phys. Chem. Chem. Phys.* **2017**, *19*, 10470–10480.
- (64) Xiong, Y.; Xu, W.; Ding, D.; Lu, W.; Zhu, L.; Zhu, Z.; Wang, Y.; Xue, Q. Ultra-Sensitive Nh₃ Sensor Based on Flower-Shaped Sns₂ Nanostructures with Sub-Ppm Detection Ability. *J. Hazard. Mater.* **2018**, *341*, 159–167.
- (65) Yang, C.; Xiao, F.; Wang, J.; Su, X. 3d Flower-and 2d Sheet-Like CuO Nanostructures: Microwave-Assisted Synthesis and Application in Gas Sensors. *Sens. Actuators, B* **2015**, *207*, 177–185.
- (66) Hao, J.; Zhang, D.; Sun, Q.; Zheng, S.; Sun, J.; Wang, Y. Hierarchical Sns₂/Sno₂ Nanoheterojunctions with Increased Active-Sites and Charge Transfer for Ultrasensitive No₂ Detection. *Nanoscale* **2018**, *10*, 7210–7217.
- (67) Yan, H.; Song, P.; Zhang, S.; Zhang, J.; Yang, Z.; Wang, Q. A Low Temperature Gas Sensor Based on Au-Loaded Mos₂ Hierarchical Nanostructures for Detecting Ammonia. *Ceram. Int.* **2016**, *42*, 9327–9331.
- (68) Gu, F.; Nie, R.; Han, D.; Wang, Z. In₂O₃–Graphene Nanocomposite Based Gas Sensor for Selective Detection of No₂ at Room Temperature. *Sens. Actuators, B* **2015**, *219*, 94–99.
- (69) Meng, F.-L.; Guo, Z.; Huang, X.-J. Graphene-Based Hybrids for Chemiresistive Gas Sensors. *TrAC, Trends Anal. Chem.* **2015**, *68*, 37–47.
- (70) Yamazoe, N. New Approaches for Improving Semiconductor Gas Sensors. *Sens. Actuators, B* **1991**, *5*, 7–19.
- (71) Qiu, H.; Pan, L.; Yao, Z.; Li, J.; Shi, Y.; Wang, X. Electrical Characterization of Back-Gated Bi-Layer Mos₂ Field-Effect Transistors and the Effect of Ambient on Their Performances. *Appl. Phys. Lett.* **2012**, *100*, 123104.
- (72) Varghese, S. S.; Lonkar, S.; Singh, K.; Swaminathan, S.; Abdala, A. Recent Advances in Graphene Based Gas Sensors. *Sens. Actuators, B* **2015**, *218*, 160–183.
- (73) Chatterjee, S. G.; Chatterjee, S.; Ray, A. K.; Chakraborty, A. K. Graphene–Metal Oxide Nanohybrids for Toxic Gas Sensor: A Review. *Sens. Actuators, B* **2015**, *221*, 1170–1181.
- (74) Yan, H.; Song, P.; Zhang, S.; Yang, Z.; Wang, Q. Dispersed Sno₂ Nanoparticles on Mos₂ Nanosheets for Superior Gas-Sensing Performances to Ethanol. *RSC Adv.* **2015**, *5*, 79593–79599.
- (75) Qiao, X.-Q.; Zhang, Z.-W.; Hou, D.-F.; Li, D.-S.; Liu, Y.; Lan, Y.-Q.; Zhang, J.; Feng, P.; Bu, X. Tunable Mos₂/Sno₂ P–N Heterojunctions for an Efficient Trimethylamine Gas Sensor and 4-Nitrophenol Reduction Catalyst. *ACS Sustainable Chem. Eng.* **2018**, *6*, 12375–12384.

- (76) Cui, S.; Wen, Z.; Huang, X.; Chang, J.; Chen, J. Stabilizing MoS₂ Nanosheets through SnO₂ Nanocrystal Decoration for High-Performance Gas Sensing in Air. *Small* **2015**, *11*, 2305–2313.
- (77) Zhang, D.; Jiang, C.; Sun, Y. e. Room-Temperature High-Performance Ammonia Gas Sensor Based on Layer-by-Layer Self-Assembled Molybdenum Disulfide/Zinc Oxide Nanocomposite Film. *J. Alloys Compd.* **2017**, *698*, 476–483.
- (78) Yan, H.; Song, P.; Zhang, S.; Yang, Z.; Wang, Q. Facile Synthesis, Characterization and Gas Sensing Performance of ZnO Nanoparticles-Coated MoS₂ Nanosheets. *J. Alloys Compd.* **2016**, *662*, 118–125.
- (79) Zhao, P.; Tang, Y.; Mao, J.; Chen, Y.; Song, H.; Wang, J.; Song, Y.; Liang, Y.; Zhang, X. One-Dimensional MoS₂-Decorated TiO₂ Nanotube Gas Sensors for Efficient Alcohol Sensing. *J. Alloys Compd.* **2016**, *674*, 252–258.
- (80) Zhang, D.; Jiang, C.; Li, P.; Sun, Y. e. Layer-by-Layer Self-Assembly of Co₃O₄ Nanorod-Decorated MoS₂ Nanosheet-Based Nanocomposite toward High-Performance Ammonia Detection. *ACS Appl. Mater. Interfaces* **2017**, *9*, 6462–6471.
- (81) Qin, Z.; Ouyang, C.; Zhang, J.; Wan, L.; Wang, S.; Xie, C.; Zeng, D. 2d Ws₂ Nanosheets with TiO₂ Quantum Dots Decoration for High-Performance Ammonia Gas Sensing at Room Temperature. *Sens. Actuators, B* **2017**, *253*, 1034–1042.
- (82) Perrozzi, F.; Emamjomeh, S.; Paolucci, V.; Taglieri, G.; Ottaviano, L.; Cantalini, C. Thermal Stability of Ws₂ Flakes and Gas Sensing Properties of Ws₂/W₃O₈ Composite to H₂, NH₃ and NO₂. *Sens. Actuators, B* **2017**, *243*, 812–822.
- (83) Jha, R. K.; Wan, M.; Jacob, C.; Guha, P. K. Enhanced Gas Sensing Properties of Liquid-Processed Semiconducting Tungsten Chalcogenide (W_xI, X= O and S) Based Hybrid Nanomaterials. *IEEE Sens. J.* **2018**, *18*, 3494–3501.
- (84) Gu, D.; Li, X.; Zhao, Y.; Wang, J. Enhanced NO₂ Sensing of SnO₂/Sns₂ Heterojunction Based Sensor. *Sens. Actuators, B* **2017**, *244*, 67–76.
- (85) Xu, K.; Li, N.; Zeng, D.; Tian, S.; Zhang, S.; Hu, D.; Xie, C. Interface Bonds Determined Gas-Sensing of SnO₂–Sns₂ Hybrids to Ammonia at Room Temperature. *ACS Appl. Mater. Interfaces* **2015**, *7*, 11359–11368.
- (86) Li, R.; Jiang, K.; Chen, S.; Lou, Z.; Huang, T.; Chen, D.; Shen, G. SnO₂/Sns₂ Nanotubes for Flexible Room-Temperature NH₃ Gas Sensors. *RSC Adv.* **2017**, *7*, 52503–52509.
- (87) Cui, S.; Pu, H.; Mattson, E. C.; Lu, G.; Mao, S.; Weinert, M.; Hirschmugl, C. J.; Gajdardziska-Josifovska, M.; Chen, J. Ag Nanocrystal as a Promoter for Carbon Nanotube-Based Room-Temperature Gas Sensors. *Nanoscale* **2012**, *4*, 5887–5894.
- (88) Mao, S.; Cui, S.; Lu, G.; Yu, K.; Wen, Z.; Chen, J. Tuning Gas-Sensing Properties of Reduced Graphene Oxide Using Tin Oxide Nanocrystals. *J. Mater. Chem.* **2012**, *22*, 11009–11013.
- (89) Cao, Q.; Dai, Y.-W.; Xu, J.; Chen, L.; Zhu, H.; Sun, Q.-Q.; Zhang, D. W. Realizing Stable P-Type Transporting in Two-Dimensional Ws₂ Films. *ACS Appl. Mater. Interfaces* **2017**, *9*, 18215–18221.
- (90) Dou, L.; Yang, Y. M.; You, J.; Hong, Z.; Chang, W.-H.; Li, G.; Yang, Y. Solution-Processed Hybrid Perovskite Photodetectors with High Detectivity. *Nat. Commun.* **2014**, *5*, 5404.
- (91) Li, C.; Han, C.; Zhang, Y.; Zang, Z.; Wang, M.; Tang, X.; Du, J. Enhanced Photoresponse of Self-Powered Perovskite Photodetector Based on ZnO Nanoparticles Decorated CsPbBr₃ Films. *Sol. Energy Mater. Sol. Cells* **2017**, *172*, 341–346.